11-27-2014

Turbidity-Based Sediment Monitoring in Northern Thailand: Hysteresis, Variability, and Uncertainty

Shawn G. Benner
Boise State University

Spencer H. Wood
Boise State University

Turbidity-based sediment monitoring in northern Thailand: hysteresis, variability, and uncertainty

Alan D Ziegler[a], Shawn G Benner[b], Chatchai Tantasirin[c], Spencer H Wood[b], Ross A Sutherland[d], Roy C Sidle[e], Nicholas Jachowski[1], Mike A Nullet[d], Lu Xi Xi[1], Anond Snidvongs[f], Thomas W Giambelluca[d,g], Jefferson M Fox[h]

[a]*Geography Department, National University of Singapore, Singapore, 1 Arts Link Kent Ridge, AS02-04021, Singapore 117568; tel +65 65166640; fax +65 6777 3091*
[b]*Department of Geosciences, Boise State University, Boise Idaho*
[c]*Department of Conservation, Kasetsart University, Bangkok, Thailand*
[d] *Department of Geography, University of Hawaii at Manoa, Honolulu, HI, USA*
[e]*Environmental Protection Agency, Athens Georgia, USA*
[f]*START Thailand & Chulalongkorn University, Bangkok, Thailand*
[g] *Hydrospheric Atmospheric Research Center, Nagoya University, Nagoya, Japan*
[h]*East-West Center, Honolulu, HI, USA*

ABSTRACT

Annual total suspended solid (TSS) loads in the Mae Sa River in northern Thailand, determined with an automated, turbidity-based monitoring approach, were approximately 62,000, 33,000, and 14,000 Mg during the three years of observation. These loads were equivalent to basin yields of 839 (603-1170), 445 (217-462), and 192 (108-222) Mg km^{-2} for the 74.16-km^2 catchment during 2006, 2007, and 2008, respectively. The yearly uncertainty ranges indicate our loads may be underestimated by 38-43% or overestimated by 28-33%. In determining the annual loads, discharge (Q) and turbidity (T) values were compared against 333 hand-sampled total suspended solid concentrations (TSS) measured during 18 runoff events and other flow conditions across the three-year period. Annual rainfall varied from 1632 to 1934 mm; and catchment runoff coefficients (annual runoff/annual rainfall) ranged from 0.25 to 0.41. Measured TSS ranged from 8-15,900 mg l^{-1}; the low value was associated with dry-season base flow; the latter, a wet-season storm. Storm size and location played an important role in producing clockwise, anticlockwise, and complex hysteresis effects in the Q-TSS relationship. Turbidity alone was a good estimator for turbidity ranges of roughly 10-2800 NTU (or concentrations approximately 25-4000 mg l^{-1}). However, owing to hysteresis and high sediment concentrations that surpass the detection limits of the turbidity sensor during many annual storms, TSS was estimated best using a complex multiple regression equation based on high/low ranges of turbidity and Q as independent variables. Turbidity was not a good predictor of TSS fractions > 2000 μm. Hysteresis in the monthly Q-TSS relationship was generally clockwise over the course of the monsoon season, but infrequent large dry-season storms disrupted the pattern in some years. The large decrease in annual loads during the study was believed to be related to depletion of fine sediment delivered to the stream by several landslides occurring the year prior to the study. The study indicated the importance of monitoring Q and turbidity at fine resolutions (e.g., sub-hourly) to capture the TSS dynamics and to make accurate load estimations in this flashy headwater stream where hysteresis in the Q-TSS signature varied at several time scales.

KEY WORDS: Soil erosion in the tropics; stream sediment dynamics; catchment management; southeast Asia; landslides

1. Introduction

Data describing sediment dynamics in river systems are useful for inferring both natural and anthropogenic degradation and landscape evolution processes within catchments, especially when complete sediment budgets

cannot be derived (Walling, 1999). These data are increasingly important for headwater catchments of mainland SE Asia where rapid land-cover/land-use change is contributing to a growing number of water quantity/quality problems in downstream areas (Forsyth and Walker, 2008; Ziegler et al., 2009b). Recent flooding in many SE Asian countries reinforces the need to understand the dynamics of discharge and sediment in tributary streams of larger rivers supporting multi-purpose reservoirs (Wood and Ziegler, 2008; Ziegler et al., 2011). Related, the ongoing and proposed dam building on the main stems of rivers and tributaries threatens to change river flows, sediment dynamics, and aquatic ecosystem functioning (Kummu and Varis, 2007; Wang and Lu, 2008; Ziegler et al., 2013). Looking ahead, the potential for future changes in catchment erosion processes and sediment delivery in response to predicted changes in landcover/landuse and climate in the region necessitates improving our baseline knowledge of river sediment dynamics (Fox et al., 2012; Sen et al., 2012).

The hydro-geomorphological consequences of forest conversion, cultivation on sloping lands, and road building have received significant attention in many countries throughout SE Asia, including Thailand (cf., Ziegler and Giambelluca, 1997; Hill and Peart, 1998; Ziegler et al., 2004; Valentin et al., 2008). Large-scale forest conversion for agriculture and intensification of steep-slope cultivation systems have accelerated erosion and mass wasting in many areas (Hurni et al., 1982; Janeau et al., 2003; Turkelboom et al., 2008; Rijsdijk, 2012). Roads, in particular, contribute disproportionally to catchment sediment budgets either directly or by triggering mass wasting events (Ziegler et al., 2001b, 2004; Cuo et al., 2006; Sidle et al., 2006; Sidle and Ziegler, 2012). Dense networks of footpaths may also be responsible for substantial runoff and erosion (Ziegler et al., 2001a). Despite widespread recognition of the importance of these sediment sources, few studies set in SE Asia have investigated sediment delivery to stream networks in headwater catchments (e.g., Chappell et al., 2004; Sammori et al., 2004; Sayer et al, 2006; Ziegler et al., 2006; Valentin et al., 2008; Sidle and Ziegler, 2010; Rijsdijk, 2012; Orange et al., 2012). Increasingly, however, work has been concerned with sediment and carbon delivery from large rivers to deltas and the oceans (e.g., Nelson, 2001; van Maren, 2007; Aldrian et al., 2008).

Only a handful of published studies report sediment loads for rivers in Thailand (Table 1). Data for several river systems have been collected for decades by the Thai Royal Irrigation Department (RID; www.rid.com). However, data for most of these rivers are available for only a few years (Table 1). The typical protocol is to sample the rivers several times during the year, with intensified sampling done during the monsoon period to develop a sediment rating curve based on discharge. For most rivers, this curve is based on fewer than 50 samples, which do not necessarily sample the largest flows. Thus, there is an unquantified uncertainty related to TSS estimates in the country, despite the professional manner in which they are consistently determined.

What is known generally is that annual catchment sediment yields vary among large Thai rivers, probably in response to differences in relief and geology, and in particular, in response to dynamic variables rainfall and land use (Table 1). Furthermore, substantial portions of annual river sediment loads are transported during large events, often occurring late in the monsoon rain season (e.g., Alford, 1992; Wood and Ziegler, 2008; Lim et al., 2012). Both the paucity and uncertainty of available data may stem, in part, from the difficulty in implementing intensive sediment monitoring programs, particularly on streams where large inter- and intra-storm variation hinders the development of reliable sediment rating curves based on discharge measurements. It also reflects limited resources—a problem in all countries.

Research worldwide has shown that rating curves are often not accurate for predicting sediment concentrations, particularly when there is a substantial hysteresis effect in the discharge-sediment relationship (Olive

and Reiger, 1985; Williams, 1989; Brasington and Richards, 2000; Lefrancois et al., 2007; Stubblefield *et al.*, 2007; Rodriguez-Blanco et al., 2010). Some of the difficulty involves collecting sufficient samples at fine time scales to make an accurate prediction. The advancement in automated turbidity-based systems provides a means of monitoring (by proxy) river sediment concentrations efficiently, and therefore, provides a means for estimating sediment loads more accurately, provided a reasonable mathematical relationship exists between turbidity and total suspended sediment concentrations (Gippel, 1995; Lewis, 1996). As such systems are automated, measurements can be made at very fine resolutions (e.g., minutely if needed).

In this study we implemented an automated turbidity monitoring approach to explore sediment dynamics and estimate total suspended solid loads in the Mae Sa River in northern Thailand. The objective was to develop a cost-effective protocol that could be used to provide reliable estimates of sediment loads in streams that may have complex discharge-sediment relationships. The sub-objectives were four-fold: (1) investigate how TSS is related to turbidity and discharge; (2) develop techniques to construct a complete suspended sediment time series from incomplete datasets of discharge and turbidity—and additionally address the limitations posed by the inability to measure turbidity values greater than 3000 NTU (the maximum limit of the sensor); (3) explore yearly sediment dynamics, with respect to management, rainfall variability, and sediment response hysteresis; and (4) estimate the uncertainty in the prediction of sediment loads. The study is part of a larger effort to understand the potential effects of changes in both climate and land-cover/land-use in the future (APN, 2012).

[Table 1]

2. Study Area

The Mae Sa River is a headwater tributary to the Ping River that flows into the Chao Phraya River, which drains to the ocean (Figure 1). In 2004, we initiated a hydro-climatic monitoring program in the 74.16 km^2 Mae Sa catchment to explore the impacts of climate and land-cover/land-use change on hydro-geomorphological processes (Figure 1). The program involved establishing three water/energy flux climate stations, 11 rain gauges, six soil moisture measurement stations, and a stream discharge monitoring station in a natural stream channel at the catchment outlet. The density of the rain monitoring gages (1 per 6.7 km^2) is one of the highest for a monitored catchment in the region. The Mae Sa River is not dammed; and flow is not regulated, although flows are affected by water extraction for irrigation and domestic use.

[FIG 1]

Land-cover in Mae Sa catchment is representative of that now found elsewhere in developing upland areas surrounding major population centers in northern Thailand. The major land cover in the catchment is still forest, but of various degrees of disturbance (62%, Figure 1). More than 20% of catchment area is now dedicated to various types of agriculture, including tree crops, floriculture, and cultivated row crops such as cabbage. An increasing amount of agriculture land has been converted to greenhouse production systems (7% of the total land), which provide high-value cash crops to lowland urban centers. Approximately ten villages are scattered throughout the basin; and urbanized or per-urbanized (e.g., contains hybrid landscapes with fragmented urban and rural characteristics) surface occupy about 8% of the total catchment land area. Some of these villages historically participated in opium cultivation (Crooker, 2005). Several tourist sites, including elephant trekking camps, resorts, and a botanical garden, are prominent points of interest within the peri-urban landscape (e.g., Sidle and Ziegler, 2010). Encroachment on the river bank and surrounding floodplain has occurred with recent land-use

intensification. Thus, the various land-used activities of these villagers, as well as resort owners, play a complex role in terms of water management and agricultural impacts in the catchment (cf. Neef et al., 2005).

Mean annual rainfall in Mae Sa catchment varies from 1200-2000 mm across an elevation range of 500-1300 m (Figure 2). Thailand is dominated by the Asian Monsoon regime that produces a distinct wet season extending approximately from late April/early May to October/November. More than 80% of the annual total falls in the wet season (Ziegler et al., 2011). Cyclones and other forms of climatic disturbances in the form of monsoon depressions and typhoons can produce large rainstorms in Ping River sub-catchments (Lim et al., 2012). In general, cyclones originating from the Western North Pacific Ocean or the South China Sea have peak activity from August to October (Wood & Ziegler, 2008). Annual catchment runoff is approximately 25-40% of the annual rainfall total. [FIG 2]

Lithology in the catchment is variable. Milled granite and gneiss (both ortho- and para-gneiss) are the dominant rocks, but phyllite, limestone, and marble are also present. Soils are mostly Ultisols, Alfisols, and Inceptisols. Shallow A horizons are typically underlained by iron-rich B horizons, 1-3 meters thick. Thick saprolite layers (> 5m) may also rest above bedrock in some locations. Mean hillslope gradient, calculated from a 30-m DEM, is 0.28 (15.4 °); the maximum is 1.54 (57°). Many of the upper sub-catchments are high relief. The channel gradient for the entire stream network in the catchment is 0.11, with short sections varying from nearly flat to > 1.

Much of the main channel of the Mae Sa river is located on relatively flat valley floors, separated by a series of large waterfalls over bedrock (cascades). The river generally flows in a singular channel that is often confined by steep topography. In some valley locations with a wide riparian zone, the channel meanders and network is affected by agriculture—previously rice cultivation and now commercial agriculture. Stream bed material in the main channel depends on location, relative to gradient. Most steep sections are composed of cobbles and boulders overlying bedrock, while other sections are sand-dominated, but overlay larger material, including bedrock. The tributaries draining the surrounding mountain slopes often have steep, narrow channels (< 1 m) and the stream beds are composed of cobbles and boulders. In reaches where the main channel flows through relatively flat valleys the surface bed material is largely sand.

Local officials believe there has been a significant increase in sediment transport in the Mae Sa River over the last couple of decades. Stream water color is typically reddish-brown during runoff events, owing to the transport of clay material that is associated with eroded iron-rich horizons of the tropical residual soils that dominate the region. Recently, several water quality studies conducted in sub-catchments indicate increased chemical and sediment loadings (Ciglash et al., 2005; 2006; Kahl et al., 2008; Sidle and Ziegler, 2010). Erosion rates as high as 80 Mg ha^{-1} y^{-1} have been reported for some steep cultivated fields (Ongprasert, 1995). Suspended sediment yield has only been estimated once in a preliminary investigation (Ziegler et al., 2011): 1075 Mg km^{-2} yr^{-1} for year 2006. During that study, maximum TSS values ranged from 1200-7600 mg l^{-1} during six monitored storms. We have also measured discharge values exceeding 30 m^3 s^{-1} during preliminary work.

3. Methods

3.1 Automated time series collection

We implemented a hybrid approach using automated turbidity and manual total suspended solid sampling to develop a continuous signal of TSS in the Mae Sa River (cf. Gippel, 1995; Grayson et al., 1996; Lewis, 1996; Bull 1997; Kronvang et al., 1997; Stubblefield et al., 2007). Turbidity is an optical property that is an indicator of the

relative clarity of water. In fresh water, turbidity is caused by the presence of suspended and dissolved matter, such as clay, silt, fine organic matter, and other microscopic organisms, organic acids, and dyes (Davies-Colley and Smith, 2001; Anderson, 2004). With automated probes, turbidity is a measure of the light scattering effect of such particles, which is a function of their size and shape. Turbidity is expressed in nephelometric turbidity units (NTU).

Not all researchers consider turbidity a suitable replacement for TSS measurements when accurate concentrations are required, for example in compliance monitoring (Riley, 1998). As with many proxies, there is a tradeoff between accuracy and the ability to obtain data at temporal resolutions finer than can be measured by hand. Several researchers have found turbidity a suitable monitoring parameter when financial and logistical constraints prevent conducting an intensive TSS monitoring program (e.g., Packman et al., 1999; Old *et al.*, 2003; Pavenelli and Pagliarani, 2002; Stubblefield *et al.*, 2007; Lewis and Eads, 2009; Williamson and Crawford, 2011). Ironically, in developing countries, the costs of the turbidity probes and data logging equipment are often prohibitively expensive. Nevertheless, fine-temporal-resolution turbidity measurements represent a means to potentially estimate long-term times series relatively accurately, compared with methods relying solely on infrequent measurements of discharge.

At our site in Mae Sa we used a self-cleaning (infrared, 90º optics) Analite (McVann Instruments, Australia) NEP-395 turbidity probe to register a continuous turbidity signal. Turbidity and stream stage were measured automatically with a data logger for a 3-year period in an unmodified cross-section of the main channel every 20-min, and also at times when stream stage changed by a 0.5-cm increment. Thus measurements were recorded at variable intervals ranging from 1-20 minutes. Each recorded value was the median of several readings taken over a period of about 45 seconds. The turbidity probe was housed inside a perforated PVC pipe (7.6 cm diameter and 2-m long), which was suspended from a walking bridge (Figure 3). This cantilever system allowed the probe to be immersed in the water column, approximately 10-20 cm below the water surface for all flow ranges (Ziegler et al., 2011). The turbidity probe was calibrated at the factory to determine values ranging from 0 to 3000 NTU. The face of the probe was cleaned several times each year to remove any material that may have prevented an accurate reading. Following most cleanings, the calibration was verified using formazin standards of known turbidity concentrations.

[FIG 3]

River stage was measured with a 7.5-psi pressure transducer and data logger (Campbell Scientific, Logan, Utah; models CR10x) (Station 434; Figure 1b). Stage was logged simultaneously with turbidity. A stage-discharge rating curve was initially determined from 37 stage-velocity-profile measurements for discharges ranging from 0.3–30 $m^3 s^{-1}$. During this period the channel profile was monitored for changes in the stage-discharge relationship resulting from changes in the river bed. Following substantial change to the channel bed in July 2006 a new rating curve was developed from an additional 19 stage-velocity-profile measurements (Figure 2b). Owing to the difficulty in sampling at high river stages, few of our stage-velocity measurements were made at discharges >10 $m^3 s^{-1}$. Thus, a high degree of uncertainty in our sediment load estimates is likely associated with high flows (cf. Navratil et al., 2011).

Lastly, minutely rainfall was recorded with tipping-bucket rain gauges (Onset, Cape Code, MA; 15.4-cm catch area) at 11 measurement locations in the catchment. Each gauge, with a calibration of 0.254 mm tip^{-1}, was dynamically calibrated to account for variable tipping rates associated with highly variable rainfall rates in the region (Calder and Kidd, 1978; Ziegler et al., 2009a).

3.2 Event-based sampling

Total suspended solid samples were determined from water samples that were hand-collected by reaching out from the stream bank near the location of the turbidity probe during the 18 runoff events in the wet seasons of 2006, 2007, and 2008 (Figure 3). A total of 333 samples were manually collected during the three-year study: 125, 107, and 101 in 2006, 2007, and 2008, respectively. Most samples (n=258) were associated with the baseflow, rising limb, peak, and falling limb of runoff hydrographs of the events—six in each of 2006, 2007, and 2008 (Tables 2, 3). The remaining samples were collected at times when a complete storm hydrograph could not be sampled.

[TABLES 2, 3]

The basin rainfall depth associated with each of the monitored events varied greatly from about 2 to 48 mm, falling within periods ranging from more than an hour to almost an entire day (Table 2). For most small events, the rainfall distribution in the 74-km^2 basin was highly variable, with many stations receiving little or no rainfall (Figure 4). Maximum 60-minute rainfall intensity for at least one location in the basin was 43 mm h^{-1} for each of two storms in 2006 (Table 2). During two other large storms (12 Sept 2006 and 4 May 2007) almost all stations recorded more than 17-20mm of rainfall, but because of disproportional rainfall durations, these events did not necessarily produce the largest event flow volumes or peaks. Nor did they necessarily produce the highest TSS concentrations (Table 3).

[FIG 4]

Owing to safety considerations in the flashy stream we were unable to sample within the stream. Additional samples were collected during baseflow conditions and/or at other arbitrary times. We elected to collect large samples (20-l) to sample for organic material in addition to determining TSS concentrations (reported in paper submitted to *Hydrological Processes*). We recognize there is an inherent bias in our TSS sampling because it was performed at one fixed location as opposed to at several locations across the stream. Another bias is that we did not use an isokinetic depth-integrated sampler. Almost certainly our TSS values for high flows (>0.5m) are underestimated by an unknown proportion because the samples were not taken from the full depth of the water column, including in the center of the stream where water velocity was highest. Thus, the samples likely did not include part of the coarse suspended fraction (sand) transported immediately above the stream bed. We do attempt to account for this bias indirectly in our load estimates.

For the determination of TSS we analyzed the entire sample not an aliquot (Gray et al., 2000). We did so by partitioning the samples into fine (<63 μm), medium (63-2000 μm) and coarse (> 2000 μm) grain size fractions by wet sieving 20-liter grab samples (Figure 3). Three 250-ml sub-samples passing through the 63-μm sieve were individually filtered through 47-mm, pre-ashed, pre-weighed, 0.7-μm Whatman GF/F glass filters. All filtered and sieved samples were oven-dried at 105ºC to a constant mass before determining concentrations. The fine suspended solid fraction was calculated as the mean of three replicates. Thus, the $TSS_{<63\mu m}$ fraction is operationally defined as the total suspended solid material between 0.7 and 63μm. We operationally define total suspended solid concentration (TSS) as the sum of the concentrations of all three fractions ($TSS = TSS_{<63\ \mu m} + TSS_{63\text{-}2000\ \mu m} + TSS_{>2000\ \mu m}$). This three part separation was used for the 2006 and 2007 data sets; TSS for 2008 was determined gravimetrically by massing replicate 250-ml samples.

Our strategy was to collect samples corresponding to various stages of the rising and falling limbs of the storm hydrographs, anticipating that a hysteresis effect would exist in the Q-TSS relationship (e.g., Olive and Reiger, 1985; Williams, 1989; Brasington and Richards, 2000; Lefrancois et al., 2007; Stubblefield et al., 2007; Rodriguez-

Blanco et al., 2010). Hysteresis occurs where there are considerable time lags between peaks of Q and TSS (Lenzi and Marchi, 2000; Walling and Webb, 1987). In general there are three types of hysteresis: (1) clockwise or positive; (2) anti-clockwise or negative; and (3) complex or figure eight. Clockwise hysteresis is associated with systems where TSS peaks on the rising limb then declines as sediment is exhausted—this phenomenon is sometimes referred to as a first-flush effect and is often found a supply-limited systems (e.g. Walling, 1974, Sidle and Campbell, 1985; Asselman, 1999; Picouet et al., 2001; Hudson, 2003; Stubblefield et al., 2007). Anti-clockwise hysteresis is characterized by the discharge peak arriving ahead of the TSS peak, for example when the sediment source is quite far from the measurement location, the main sources are valley slopes rather than the stream system, and/or the supply of sediment in the stream does not become exhausted (e.g., Walling and Webb, 1981; Lawler, et al., 2006). Complex hysteresis patterns are marked by changes between clockwise and anticlockwise hysteresis, over various time scales (e.g., Hodgkins, 1996; Singh et al., 2005; Alexandrov et al. 2007; Duvert et al., 2010). In fact, all types of hysteresis patterns may occur over a range of intra-event, inter-event, daily, seasonal, annual, and very long-term time scales.

3.3 TSS rating curve development

In this work we move beyond developing a standard linear or non-linear approach of estimating TSS based on one predictive variable, for example of the form: $TSS = aQ^b$ or $TSS = aT + b$, where a and b are determined from regression analysis using empirical data. Instead, we endeavored to build a TSS rating curve with two independent variables, discharge and turbidity, following the form: $TSS = aQ^b + cT^d$. To do so we used the solver optimization program in Excel (Microsoft, Inc.) to reduce the error of the fit, which was assessed with the Nash-Sutcliffe (1970) model efficiency (ME) coefficient:

$$ME = 1 - \frac{\sum_{i=1}^{n}(O_i - P_i)^2}{\sum_{i=1}^{n}(O_i - \bar{O})^2} \quad (1)$$

where O_i is an observed value; P_i is a predicted value; $\bar{\boldsymbol{o}}$ is the mean of the observations. Values of ME range from minus infinity (poor model) to 1.0 (perfect model). Negative values of ME indicate that the observed mean is a better predictor than the model; a value of zero indicates that the observation mean is as good a predictor as the model (Legates and McCabe, 1999).

4. Turbidity – TSS linkage

The monitored storm events represented a wide range of flow conditions. Initial flow (Q_i) at the commencement of sediment sampling ranged from 0.6 to 8.0 $m^3\ s^{-1}$; and peak flows (Q_p) ranged from 1.2 to 29.7 $m^3\ s^{-1}$ (Table 3). Streamflow was flashy, with discharge peaks rarely lasting an hour. Peaks typically arrived at the recording station within 1-2 hours for storms located in the central and/or lower part of the catchment (e.g., 8 and 9 August 2006). Peaks associated with storms in the upper catchment typically occurred 2-3 hours after peak rainfall (e.g., 28 August 2007). For these "distant" storms, for example the event on 3 June 2008, peak TSS was delayed by an hour or more, contributing to a counter clockwise hysteresis effect (Figure 5). Measured TSS for the entire data set ranged from 8 to 15,906 mg l^{-1}. Meanwhile, turbidity ranged from 1 to 3000 NTU. (Table 3). The upper value of this range was the maximum value outputted from the turbidity probe. A total of 29 of the 333 manually collected water

samples had turbidity values of 3000 NTU; the corresponding sample TSS values ranged from 2972-15906 mg l^{-1}. Thus, there was a large range of TSS concentrations that were not approximated well with turbidity as a proxy. For the 18 monitored events, turbidity reached 3000 NTU in six. Low concentration situations were also problematic because detection on the low end was compromised by calibrating the probe to register across a wide range of turbidities. Thus turbidity values of zero (below detection limit) corresponded with TSS values ranging from 8-22 NTU. For cases of turbidity = 0 NTU, we changed the turbidity values to 1 NTU to facilitate graphing and regression analysis. Nevertheless, we stress that turbidity was a good predictor of TSS (R^2 = 0.87) when turbidity values fell in the range of 5-2800 NTU, and corresponding TSS ranged from 30-5000 mg l^{-1} (Figure 6).

[FIG 5,6]

The maximum measured suspended solid concentration (15,906 mg l^{-1} at Q = 5.66 m^3 s^{-1}) occurred on the falling limb of the 11 June 2008 storm event (Table 3; Figure 5). Notably, other samples collected at much higher flow volumes had substantially lower TSS values: e.g., 5,560 mg l^{-1} at Q = 21.35 m^3 s^{-1} on 12 Sept 2006; and also TSS = 7660 mg l^{-1} for Q = 15.35 m^3 s^{-1} during the same event (Figure 5). Conversely, high TSS values were occasionally recorded at relatively low discharges: e.g., 6,250 mg l^{-1} at Q = 2.32 m^3 s^{-1} during the 14 June 2007 event. The inconsistent relationship between Q and TSS is, in part, the result of marked within-storm hysteresis in the Q-TSS relationship (Figure 5). While there is substantial scatter in the plot of Q versus TSS, the plots of Q versus turbidity have even more scatter because of the limitation of the turbidity probe having an maximum detection of 3000 NTU (Figure 7). If the three size fractions are considered, the best predictive relationship existed between turbidity and the <63μm fraction (Figure 8). Substantial scatter existed between turbidity and the two larger fractions; and discharge was not a good predictor for any of the three fractions (Figure 8). Great inter- and intra-storm variation between Q and TSS portends that a sediment rating curve based solely on discharge would be inaccurate (cf. Lopes and Ffolliott, 1993; McBean and Al-Nassri, 1988).

[FIGS 7,8]

5. Construction of long-term TSS time series

For the construction of the long-term total suspended solids times series we focused on all size fractions combined, largely because we did not have size fraction data for 2008, but also because of the poor relationship between the largest fraction and both discharge and turbidity. We also needed to estimate the total range of observed TSS concentrations (8-16,000 mg l^{-1}); therefore, the simple exponential equation shown in Figure 6 could not be used.

Because of the observed hysteresis the model efficiency of the best-fit non-linear regression equation between TSS and Q alone for combined years 2006-2008 was only 0.48 (Figure 9a):

$$TSS_{2006\text{-}08} = -11.26Q^2 + 544.38Q \quad (2)$$

[Figure 9]

The best-fit equation using turbidity (T) alone was substantially better (ME = 0.63; Figure 9b):

$$TSS_{2006\text{-}08} = 1.502T \quad (3)$$

Better fit for Eq. 3 was not surprising because turbidity has provided reasonable sediment concentration estimates elsewhere (e.g., Brasington and Richards, 2000; Gippel, 1995; Langlois *et al.*, 2005; Pavanelli and Pagliarani, 2002; Stubblefield *et al.*, 2007). Again, we found a really strong relationship between turbidity and TSS alone for a subset of the range of concentrations observed in the stream (Figure 6). However, Eq. 3 has difficulty in fitting TSS accurately over a range spanning several orders of magnitude (Figure 9b), in particular, when T > 3000 NTU—because this value is the upper limit of the turbidity sensor we used in the study.

Thus, a complicating factor in our study is the large range of observed sediment concentrations (8-16,000 mg l^{-1}) that are paired with a smaller range of turbidity values (0-3000 NTU). In recognizing that high values of turbidity often coincided with high discharge, multiple linear regression using both Q and T was attempted, but resulted in only a slightly better fit (ME = 0.69; Figure 9c):

$$TSS_{2006\text{-}08} = 136.67Q + 1.13T \quad (4)$$

Equation 4 also has difficulty fitting TSS spanning several orders of magnitude (Figure 9c). An improvement to fit across the entire range of values was attempted with a complex, non-linear model that breaks the data into two turbidity ranges:

$$\text{TSS (mg l}^{-1}) = \begin{cases} aT^b & T \leq 200 \text{ NTU} \\ cQ^d + eT^f & T > 200 \text{ NTU} \end{cases} \quad (5)$$

where coefficients a, b, c, d, e, f were determined with an optimization program that maximized model fit. A turbidity value of 200 NTU was a good threshold for this break probably because the turbidity probe was calibrated over a large range (0-3000) as opposed to a smaller range (0-100 NTU).

The best-fit equation for all data collected in 2006-2008 resulted in a model efficiency of ME = 0.73 (Figure 9d):

$$TSS_{2006\text{-}08} \text{ (mg l}^{-1}) = \begin{cases} 8.112T^{0.62} & T \leq 200 \text{ NTU} \\ 342.23Q^{0.68} + 0.00003T^{2.36} & T > 200 \text{ NTU} \end{cases} \quad (6)$$

Better fits were obtained when separate equations were derived for each individual year (ME = 0.90, 0.75, and 0.75; Figure 9e,f,g):

$$TSS_{2006} \text{ (mg l}^{-1}) = \begin{cases} 9.963T^{0.60} & T \leq 200 \text{ NTU} \\ 99.981Q^{1.15} + 0.2795T^{1.15} & T > 200 \text{ NTU} \end{cases} \quad (7)$$

$$TSS_{2007} \text{ (mg l}^{-1}) = \begin{cases} 11.02T^{0.56} & T \leq 200 \text{ NTU} \\ 347.66Q^{0.98} + 0.0004T^{1.99} & T > 200 \text{ NTU} \end{cases} \quad (8)$$

$$TSS_{2008} \text{ (mg l}^{-1}) = \begin{cases} 9.93T^{0.50} & T \leq 200 \text{ NTU} \end{cases} \quad (9)$$

$$99.91Q^{1.29} + 0.000005T^{2.60} \qquad T > 200 \text{ NTU}$$

The robustness of these equations in estimating the TSS signal, for which more than half the values exceeded the turbidity threshold at 200 NTU, can be seen in Figure 9e-h.

The following complex equation, which incorporates Eqs. 2, 3, 7, 8, and 9, was used to estimate annual loads from the average hourly time series for years 2006, 2007, 2008:

$$TSS_{year}(\text{mg L}^{-1}) = \begin{cases} 8 & \text{if } TSS_{predicted} \leq 8 \\ \text{Eq. 7,8, or 9} & \text{if Q and T are available} \\ \text{Eq. 3*} & \text{if Q is missing} \\ \text{Eq. 2*} & \text{if T is missing} \\ 16{,}000 & \text{if } TSS_{predicted} \geq 16000 \end{cases} \quad (10)$$

For any given year (2006, 2007, or 2008), Eq. 10 uses the year-specific versions of Eqs. 7, 8, or 9 to estimate TSS when Q and T are available. In cases where one variable is missing, year-specific variations of Eqs. 2 or 3 were substituted (indicated by '*'; individual equations are not shown). Finally, estimated TSS was restricted to fall within the approximate range of observed values for the whole period (i.e., 8-16,000 mg l^{-1}). The model fit (ME = 0.78) for the three-year period was intermediate of each individual yearly model (Figure 9h). The annual load calculations included six periods of with relatively high error levels caused by missing turbidity data (Figure 10): 15-21 May 2006; 25-26 July 2006; 17 Dec 2006 – 1 Jan 2007; 22-23 Aug 2007; 1 Jan – 27 April 2008; 29 Oct – 8 Nov 2008; 8 Nov – 31 Dec 2008. All gaps (19% of the time series) were addressed using Eq. 2* in Eq. 13, as described above.
[Figure 10]

6. Uncertainty

All aspects of predicting sediment loads from discharge- and turbidity-based rating curves have associated error and uncertainty (Walling, 1977; Crawford, 1991; Navratil, et al., 2011; Skarbovik et al., 2012). A large part of this uncertainty can be represented by the following equation that recognizes that the overall uncertainty (ξ) is a function of the combined uncertainties of many measurements:

$$\xi = f(\xi_{stage}, \xi_Q, \xi_T, \xi_{TSS}, \xi_{agg}) \quad (11)$$

where ξ_{stage} represents the error in determining the mean stage across the channel at any given time (based on a relationship between water depth and pressure at the stilling well); ξ_Q is aggregated error in determining stream discharge from a rating curve based on water depth and a limited number of hand-measurements. The measurement of turbidity with a probe has a small error (ξ_T) related to resolution and repeatability of the instrument. Each TSS measurement has error (ξ_{TSS}) associated with failure to collect appropriate depth-integrated samples from across the stream, as well as other errors while handling and processing the samples. Once the TSS prediction

equation has been determined, it will typically only explain about 70-90% of the variance in the observed signal. In computing a sediment load one often aggregates instantaneous readings to manageable time steps (e.g., minutely Q and T measurements to hourly values) to make the calculation tractable. Such aggregation acts to smooth the signal, for example short-lived spikes in sediment concentration are often eliminated. Determination of the final value of ξ in Eq. 11 is not simply additive, as some of the errors are inter-related, some propagate as the long-term times series is computed, and some may offset each other. Many are difficult to isolate without conducting specific measurements under a range of experimental conditions (Navratil, et al., 2011). Many of these measurements are difficult to do in the field under stormy, and sometimes dangerous, conditions.

In estimating uncertainty in this study we simplified equation 11 to the following:

$$\xi_i = f(\xi_{Qi}, \xi_{T\text{-}TSSi}) \tag{12}$$

where the estimation error or uncertainty at any time stamp i (ξ_i) is determined by the uncertainty in the measurement of instantaneous discharge (ξ_{Qi}) and uncertainty in relationship between measured turbidity and instantaneous total suspended solids ($\xi_{T\text{-}TSSi}$). All are expressed as percentages. The first term subsumes the errors stated above related to the measurement of stage and determination of discharge from the rating curve. In the comparison of our measured discharge calculations at periods with similar measured depths (19 "pairs"), the median difference was 14%; this represents our initial estimate of ξ_{Qi}. However, because we have so few data points for high flows, this value is likely an underestimate of the uncertainty at the high range of flows, which we assume to be on the order of 20%. We therefore estimate ξ_{Qi} with the following equation:

$$\xi_{Qi} = 0.15Q_i^{0.7} \tag{13}$$

where Q_i is instantaneous discharge varying over a range of 0.5 to 65 $m^3\ s^{-1}$. In equation 13, ξ_{Qi} ranges from 14-20%.

The term ξ_{TSSi} in Eq. 12 incorporates all errors associated with estimation of instantaneous total suspended solids from turbidity measurements. When we compared our measured TSS (n=333) with TSS (calculated from Eq. 10), the residuals (%) did not display an obvious trend related to the magnitude of measured sediment concentrations (i.e., for different bins sizes). Surprising, the baseflow estimate errors were higher than those for storm flows (37% versus 24%), but this could be an artifact of only having a handful of baseflow estimates and a wide range of TSS concentrations (8 to 22 mg l^{-1}). Uncertainty was however distinctly different for each year of consideration. Thus, in the calculation of uncertainty for the sediment load estimations in this paper we used the following percentages for various conditions: 37% (all baseflows); 18% (2006 storm flow data); 27% (2007 storm flow data); 28% (2008 storm flow data). Further, owing to the likely bias in our sampling method, we increase the uncertainty an additional 10% for high energy flows that would have higher concentrations of sand in suspension ($Q > 5\ m^3\ s^{-1}$). Admittedly, this ad hoc adjustment has little supporting data, but we feel it is necessary to include it because of the almost certain under-sampling of sand during the measurements of TSS from which the rating curse was developed. In the calculation of the annual sediment load we first estimate minimum and maximum discharges

for a given time stamp using the "error" term derived from Eq. 13. These discharge rates are then used in the calculation of TSS (from Eq. 10), for which upper and lower uncertainty bands are determined.

7. Annual total suspended solid dynamics and loads

Estimated annual sediment loads for 2006, 2007, and 2008 were approximately 62,200 (range = 44,700-86,700), 23,900 (16,000-34,300), and 11,900 (8,000-16,400) Mg, respectively (Figure 10; Table 4). These loads are equivalent to basin yields of 839 (603-1170), 323 (217-462), and 160 (108-222) Mg km^{-2} y^{-1} (Table 4). The ranges in parentheses represent uncertainties (over- and under prediction) of 28 to 39%, 33 to 43%, and 33 to 38% for the three respective years (Table 4). The 2006 sediment load and yield values reported here supersede higher preliminary values reported by Ziegler et al (2011). Again, we attempted to correct for the likely underestimate of TSS owing to the bias in our sampling, which underestimates sand proportion. However, without extensive new data we cannot substantiate this correction. It may be the case that the upper bounds for annual sediment loads are even higher than we report here.

The range of total suspended solids yields is high compared with several other northern Thailand rivers (Table 1; Figure 11). Only three rivers had mean/median TSS yields higher than what we determined for Mae Sa (median = 323 Mg km^{-2} y^{-1}; Table 1): the Lai (947 Mg km^{-2} y^{-1}); the Nan (391 Mg km^{-2} y^{-1}) and the Pat (383 Mg km^{-2} y^{-1}), a Nan River tributary. Also, only five rivers had maximum reported sediment yields higher than our highest value for Ma Sa (839 Mg km^{-2} y^{-1} in 2006): the Yom (3652 Mg km^{-2} y^{-1}); the Nam Khuan (2632 Mg km^{-2} y^{-1}); the Lai (2629 Mg km^{-2} y^{-1}), the Wang (1108-1950 Mg km^{-2} y^{-1}), and the Nan at Tha Wang Pha (1215 Mg km^{-2} y^{-1}). The relatively high yields in Mae Sa are not surprising given the small size of the catchment compared with those of larger river systems where storage of eroded soil within the catchment is potentially greater, and sediment delivery ratios may be significantly smaller. They are also not surprising given that the measurement procedures for the other rivers/streams involves comparatively less sampling to determine the sediment rating curves. Interesting, however, is that TSS yields in Ma Sa should be even higher than our estimates because of the inherent bias in our sampling strategy, which under-samples the coarser fractions.

[Table 4]

[Figure 11]

Annual precipitation and basin runoff were also very different across the three years. For example, rainfall was approximately 300 mm higher in 2006 than the ~1600mm falling in 2007 and 2008 (Table 4). Consequently runoff coefficients (discharge/rainfall) decreased from 0.41 in 2006 to 0.34 and 0.25 in the 2007 and 2008. Total suspended solid loads are largely determined by total rainfall and storm characteristics, but other catchment conditions also contribute to load differences. The higher load measured in 2006 versus subsequent years was, in part, caused by 300 mm more runoff, which was caused by greater rainfall (Table 4). There were also nine large (peak hourly discharge > 20 m^3 s^{-1}) runoff events in 2006, compared with only two in 2007 and none in 2008 (Figure 10). Six events in 2006 had peak estimated TSS values > 10000 mg l^{-1}; only one in 2007; and none in 2008. Channel bed and bank erosion may have been greater in 2006 than the other years; however, we did not quantify this.

Obvious in the annual time series is the distinct seasonality in sediment transport related to the timing of the monsoon wet season, typically mid-May through October/November (Figure 10). Most of the rainfall and discharge (70-80%) take place during this period. Similarly most of the total suspended solid load (80-90%) occurs during months with large storm activity. For example, several large events are noticeable in the 2006 time series

(Figure 10). Worldwide, large events are often responsible for disproportional contributions of sediment to annual loads, particularly if significant erosion or mass wasting occurs (Collins and Walling, 2004; Chappell et al., 2004; Duvert et al., 2010). Various conditions in Mae Sa catchment also contributed to changes in sediment loads over time. For example, several road-related landslides occurred throughout the catchment in 2005, generating an estimated 60,000 Mg of material that remained on or near the road-side margin (Ziegler, unpublished data). Observations support that this material was gradually transported to the stream system during subsequent storm events occurring over the next few years. In many instances, high concentration sediment plumes could be tracked to landslide debris source areas. The initially high TSS load observed in 2006 may have been elevated by transport of some of this landslide material. However, it could also be explained by excavated and graded areas left barren by construction projects in the riparian zone. The reduction in observed sediment load in 2007 and 2008 may therefore have been related to depletion of supply – as well as less rainfall and fewer intense storms.

A clockwise annual hysteresis pattern in the discharge-total suspended solid load relationship occurred over the course of some years, as clearly shown for 2006 (Figure 12). The clockwise direction, which is indicative of flushing of material on the rising limb of the annual hydrograph, results from the monsoon rainfall regime, for which river discharges generally increase until the end of the rainy season, particularly in larger rivers. Discharge then decreases steadily until the next wet season. A less obvious hysteresis pattern was observed for 2007 and 2008, as large storms in the early dry season produced high sediment loads in months when discharge was comparatively low (e.g., March and May, 2007). High loads may also have been caused by construction to re-enforce the eroding channel bank at a meander near the road (Jan 2007). Obvious in Figures 10 and 12 is the reduced discharge in 2007 and 2008, which undoubtedly contributed to the lower corresponding total suspended solid load, as compared with 2006 loads.

[Figure 12]

8. Storm variability

Just as better fit for the sediment curves could be achieved using data from each individual year, the best predictive equations for TSS for each storm were derived from individual storm data alone. Model efficiency values ranged from 0.63 to 0.99; and most were above 0.70 (Table 5). The fit for all equations is generally good except for a few peaks (e.g., 060909) and falling limbs (e.g., 080523; Figure 13). The storm time series on 080611 was in particular not estimated well. Total suspended solid loads calculated from measured Q and T for each of the 18 storms ranged from 6 to 788 Mg (TSS_{load}, Table 3). Uncertainty in these estimations range from ±26-41% (Table 5). Despite under predicting the highest concentrations in the largest event (080611), TSS_{load} from this storm comprised 7% of the total load for Mae Sa River in 2008 and was transported in only 0.3% of the time, demonstrating the importance of singular large events in sediment transport.

[Table 5; Figure 13]

Again, various types of hysteresis patterns in the discharge/sediment relationship are commonly reported worldwide (e.g., Asselman, 1999; Jansson, 2002; Hudson, 2003; Sammori et al., 2004; Singh et al., 2005; Coynel et al., 2005; Lawler et al., 2006; Smith and Dragovich, 2009; Xu and Milliman, 2009; Oeurng et al., 2010; Duvert et al., 2010; Beel et al., 2011; Fang et al., 2011). We observed more than one dominant type during the 18 monitored events (Figure 5). Seven of 13 observed cases were of the anticlockwise type; and they usually occurred for small- to medium-sized events where peak discharge was < 6 m^3 s^{-1}. Large storms tended to produce complex or clockwise

hysteresis relationships (Figure 5). Small storms often did not show hysteresis or demonstrated an uncertain pattern—lack of a clear pattern may also be related to under-sampling.

Hysteresis is inherently related to the size and shape of the catchment, the location of sediment sources, factors affecting sediment availability, hydrological pathways, and flowpath linkages (Lawler et al., 2006; Duvert et al., 2010). Anticlockwise patterns in Mae Sa occurred when the sediment originated from distant upland agriculture areas, as can be seen by comparing storm 060908 patterns in Figures 4 and 6. It may also be caused when the bulk of the fine transportable sediment is stored temporarily in the lower reaches of the floodplain and does not get inundated until the peak of the storm event, and thus not transported downstream until the falling limb. A clockwise pattern is caused by the sediment peak arriving before the discharge peak. We believe events in Mae Sa with this pattern were those where the front edge of the discharge wave entrained material that had been stored in the stream channel during prior events. Sediment transport decreased once the easily entrained, stored material was depleted and transport capacity of the stream decreased. The occurrence of this phenomena is plausible given the relative flatness of the lower portion of the basin (allowing storage), compared with the upper reaches where most hillslope erosion occurs (assuming channel bank and bed erosion is small). Intense rainfall in the lower portion of the catchment can initiate this response (e.g., storm 070823; Figures 4,6). Complex hysteresis signals were caused by the consecutive arrival of runoff water from isolated and distant locations in the catchment, having different total suspended solid concentrations. Rainfall throughout the catchment (e.g., storm 070614; Figures 4,6) therefore produced a hybrid signal that was composed of the entrained material stored in the channel (i.e., typically caused clockwise hysteresis) and sediment transported from distant erosion sources (produced anticlockwise hysteresis).

Our data and observations suggest that because of an inherent connection between storms and the characteristics of TSS comprising the storm sedigraph (cf. Alexandrov *et al.*, 2007; Sammori *et al.*, 2004), knowledge of the spatial distribution of rainfall during individual storms could be exploited to generate better TSS estimations from continuous turbidity signals. As shown in Figure 14, samples collected during high concentration peaks of three sampling events had very different particle size distributions (Clifford *et al.*, 1995). The color of the material also indicates they come from different sources of eroded material. As particle size greatly affects the turbidity signal (Landers and Sturm, 2013), the different materials, including organic matter, have substantially different turbidity-TSS relationships (Figure 14). The range of total suspended solid concentrations for a corresponding turbidity reading is so large that an individual regression model would have great uncertainty.

[Figure 14]

The first peak (E1) of the larger event was associated with rainfall on nearby forested sources where several trails contributed runoff (Sidle and Ziegler, 2010). The second peak (E2) originated from rainfall in an area where a large debris flow had occurred earlier in the year (Figure 14). Note that these data are from a pilot study in 2005, and are not shown in the figures and tables above. The first event remobilized in-stream material near the basin outlet causing a clockwise hysteresis effect; the latter, fine material from the clay-rich subsoils in higher sections in the catchment, causing a shift to a counter-clockwise hysteresis effect. The third peak (E3) occurred during a storm four days later in a high-elevation agricultural subcatchment. These differences suggest that unique turbidity/TSS rating curves based on rainfall location, which is a proxy for a sediment source, could be used to develop a group of sediment rating curves to provide a more accurate continuous TSS estimate than a single equation. This approach is analogous to developing separate curves based on seasonality.

9. Sediment size fractions

The sediment fraction data we collected for the 12 storms in 2006 and 2007 allowed us to estimate the contribution of each to the total loads of these storms. To do so, we determined best-fit non-linear regression equations for each the three fractions following the form of equation 6 (individual equations are not shown). Simulated versus predicted TSS for the <63 μm, 63-2000 μm, and > 2000 μm fractions are shown in Figure 15; and the estimated totals for the 12 events in 2006 and 2007 are listed in Table 3. The approach did well in predicting the smallest fractions, but not the coarse fraction (Figure 15). For example, ME values for the 060724 event were 0.99, 0.83, and 0.19, respectively for the <63 μm, 63-2000 μm, and > 2000 μm fractions (goodness-of-fit ME values for other events are not shown).

[Figure 15]

The <63 μm was always the greatest except for the largest monitored event (060912), when the 63-2000-μm fraction comprised 50% of the load. The maximum contribution of the <63 μm fraction was 95%, occurring during a medium-sized event (060808). The 63-2000 μm fraction ranged from 4-50%; and it was usually less than half that of the <63 μm fraction. In 2006, material <63 μm comprised on average 64% of the load, compared with 35% and 1% for the 63-2000 μm and > 2000 μm fractions (Table 3). In 2007, the <63 μm fraction was higher (72%). The 63-2000 μm and > 2000 μm fractions were 27 and 1%, respectively. The difference between the two years could be the result of higher flows in 2006 moving slightly larger material. It might also be related to greater availability of the intermediate material, for example, that from landslides or channel bank erosion. Finally, we admit these results are preliminary, as the large fractions are likely underestimated owing to the bias in our sampling method (see above).

10. Conclusion and implications

The processes occurring throughout the Mae Sa catchment contributing to sediment loads are numerous and occurring across several spatio-temporal scales. While chronic sources of soil material entering streams may exist (e.g., road cuts or agricultural fields), other sources might be short-lived, such as infrequent mass wasting events or in-channel construction. Ever-changing loads could also be related to natural processes such as variation in channel bank and channel bed erosion in response to variability in storm intensity and stormflow generation. In addition, the observed mass wasting may have dumped sediment into a stream channel causing aggradation, and changes to bed slope, but this could not be quantified. In basins such as Mae Sa, where the spatial distribution of rainfall is highly variable and streamflow is flashy, the arrival of sediment from distant, isolated sources is easy to miss if sampling is insufficient. Had we not used an automated approach that measures both discharge and turbidity at fine time resolutions, we would have likely failed to obtain realistic portrayal of sediment dynamics. The great inter- and intra-storm variability in sediment transport, as well as the varying types of hysteresis observed, demonstrates the need to monitor discharge and total suspended solid concentrations at fine temporal resolutions to produced accurate load estimates (Duvert et al., 2011). Further, the five-fold range in annual sediment load also demonstrates the need to begin monitoring more tributary streams continuously if accurate estimates are to be made of sediment transported to larger, managed rivers and/or downstream reservoirs in the country. Few small catchments in Thailand are monitored sufficiently to provide reliable information of rainfall, runoff, and sediment transport relationships for management purposes.

Our objective was to develop a better method of constructing a long-term total suspended solid time series for calculating annual loads than a simple discharge-based rating curve (Jastram et al., 2010). Our automated turbidity and discharge measurement approach allowed this, but we encountered several layers of uncertainty, related to the measurement of all variables. Importantly, the low range of the turbidity probe (0-3000 NTU) compared with the high range of concentrations of total suspended sediment (8-15,906 mg l^{-1}) hindered development of a simple TSS prediction equation. A non-linear multiple regression approach using both discharge and turbidity performed reasonably well in the system with complex hysteresis patterns in the Q/TSS relationship; however, portable turbidity probes capable of determining values that exceed 10,000 to 15,000 NTU would have been beneficial. Nevertheless, for relatively low TSS concentrations (<3000-4000 mg l^{-1}), a good predictive relationship using turbidity alone could be established.

The uncertainty in our annual estimates (underestimated by 38-43% or overestimated by 28-33%) is not unreasonable for a river with large variability in hysteresis in the suspended solid–discharge relationship. In the 18 monitored storms, we encountered all of clockwise, counter-clockwise, and complex hysteresis patterns. Despite uncertainty, we believe this automated method of estimating the total suspended load is better than one that relies solely on a discharge-based sediment rating curve because the relationship between these two variables is very poor. As a simple demonstration in support of this assertion, several discharge-based rating curves created from 50 randomly selected data pairs (Q, TSS) from our 2006-2008 dataset, over-estimated our load annual load predictions by 33 to 118% (cf. Duvert et al., 2011). Underestimates are also possible. The largest uncertainty in our estimates stems from an inherent bias in our sampling scheme that likely under-sampled the coarse fractions in the TSS values used to build the rating curve. Others certainly want to avoid this limitation in the future through proper sampling.

The remaining question is whether this approach is a feasible for operational use in developing countries by entities charged with monitoring sediment loads. The initial set-up costs alone may be on par with the annual salaries of two to three employees; and the long-term maintenance may be equivalent to that of one more. These costs alone are probably restrictive. Our finding that the best estimates are based on equations developed from data collected annually necessitates having a dedicated, complementary river monitoring program that samples across storms, rather than one that collects a handful of samples at discrete points in time, which is the typical practice. This sampling is needed to collect Q and total suspended solid concentration data associated with all types of hysteresis that vary from storm to storm, and importantly, prevents the use of a simple discharge-based equation (Gippel, 1999). Despite great effort each of the three years of the study, we were only able to sample 6 storms, which contributed 1.5%, 4.0%, and 8.3% of their respective annual loads. Failure to sample a larger proportion of the total flows likely adds to the uncertainty in our estimates. Thus, the amount of time required to produce an "accurate" estimate of sediment loads from this approach—despite it being automated—may prevent its adoption, except for scientific study. Finally we caution against placing too much confidence on the load/yield estimates made for small catchments such as Mae Sa using automated measurements of discharge alone. Errors associated with those estimates must be greater than or equal to the ones we determined for Mae Sa (up to 43%).

Acknowledgements

This project was supported by SARCS grant 95/01/CW-005; APN grants #ARCP2006-06NMY, #ARCP2007-01CMY & #ARCP2007-01CMY; NASA grant NNG04GH59G, and NUS grant R-109-000-092-133. A special thanks is given to Ms. Wimonmat Nuipakdee (Department of National Park, Wildlife and Plants Conservation,

Thailand) for providing access to the research site. This document has been reviewed in accordance with U.S Environmental Protection Agency policy and approved for publication. Mention of trade names or commercial products does not constitute an endorsement or recommendation for use.

References

1. Aldrian, E., Chen, C.-T.A., Adi, S., Prihartanto, N., Sudiana, N., Nugroho, S.P. 2008. Spatial and seasonal dyanmics of riverine carbon fluxes of the Brantas catchment in East Java. Journal of Geophysical Research 113, G03029, doi: 10.1029/2007/JG000626.
2. Alexandrov, Y., Laronne, J.B., Reid, I. 2007. Intra-event and inter-seasonal behavior of suspended sediment in flash floods of the semi-arid northern Negev, Israel. Geomorphology 85, 85-97.
3. Alford, D. 1992. Streamflow and sediment transport from mountain watersheds of the Chao Phraya Basin, Northern Thailand: a reconnaissance study. Mountain Research and Development 12, 257-268.
4. Al-Soufi, R. 2004. Soil erosion and sediment transport in the Mekong basin. In: Proc. of 2nd APHW conference, Singapore, pp. 47–56
5. Anderson, C.W. 2004. Turbidity. Book 9, chapter, A6, section 6.7. In National Field Manual for Collectin of Water-Quality Data. U.S. Geological Survey Techniques of Water-Resources Investigations. USGS: USA.
6. Asia-Pacific Network for Global Change Research (APN). (2012). Sediment Dynamics and Downstream Linkages in Tropical Streams as Affected by Projected Land-Cover/Land-Use and Climatic Change. Retrieved from http://www.apn-gcr.org/resources/items/show/1541
7. Asselman, N.E.M. 1999. Suspended sediment dynamics in a large drainage basin: the River Rhine. Hydrological Processes 13, 1437-1450.
8. Beel, C.R., Orwin, J.F., Holland, P.G. 2011. Controls on slope-to-channel fine sediment connectivity in a largely ice-free valley, Hoophorn Stream, Southern Alps, New Zealand. Earth Surface Processes and Landforms 36, 981-994.
9. Brasington, J, Richards, K. 2000. Turbidity and suspended sediment dynamics in small catchments in the Nepal Middle Hills. Hydrological Processes 14, 2559-2574.
10. Bricquet, J.P., Janeau, J.L., Boonsaner,A., Huon, J.P.L., Boulais, C., Lestrelin, G., Kurian, M. 2004. Catchment approach to combating soil erosion in thailand. Downloaded 16 Feb 2013 from www.publications.iwmi.org/pdf/h037208.pdf
11. Bull, L.J. 1997. Magnitude and variation in the contribution of bank erosion to the suspended sediment load of the River Severn, UK. Earth Surface Processes and Landforms 22, 1109–1123.
12. Calder, I.R., Kidd, C.H.R. 1978. A note on the dynamic calibration of tipping-bucket gauges. Journal of Hydrology 39, 383–386.
13. Chappell, N.A., Douglas, I., Hanapi J.M., Tych, W. 2004. Sources of suspended sediment within a tropical catchment recovering from selective logging. Hydrological Processes 18, 685-701.
14. Ciglasch, H., Amelung, W., Totrakool, S., Kaupenjohann, M., 2005. Water flow patterns and pesticide fluxes in an upland soil in northern Thailand. European Journal of Soil Science, 56, 765–777.
15. Ciglasch, H., Busche, J., Amelung, W., Totrakool, S., Kaupenjohann. M., 2006. Insecticide dissipation after repeated field application to a northern Thailand ultisol. Journal of Agricultural and Food Chemistry, 54, 8551–8559.
16. Clifford, N.J., Richards, K.S., Brown, R.A., Lane, S.N. 1995. Laboratory and field assessment of an infrared turbidity probe and its response to particle size and variation in suspended sediment concentration. Hydrological Sciences Journal 40, 771–791.
17. Collins, A.J, Walling, D.E. 2004. Documenting catchment suspended sediment sources: problems, approaches and prospects. Progress in Physical Geography 28, 159-196.
18. Crawford, C.G. 1991. Estimation of suspended-sediment rating curves and mean suspended-sediment loads. Journal of Hydrology 129, 331-348.
19. Crooker, R.A. 2005. Life after Opium in the hills of Thailand. Mountain Research and Development 25, 289-292.
20. Cuo, L., Giambelluca, T.W., Ziegler, A.D., Nullet, M.A. 2006. Using Distributed-Hydrology-Soil-Vegetation Model to study road effects on stream flow and soil moisture. Forest Ecology and Management 224, 81-94.
21. Coynel, A., Seyler, P., Etcheber, H., Meybeck, M., Orange, D. 2005. Spatial and seasonal dynamics of total suspended sediment and organic carbon species in the Congo River. Global Biogeochemical Cycles 19, DOI: 10.1029/2004GB002335.
22. Davies-Colley, R.J., Smith, D.G. 2001. Turbidity, suspended sediment, and water clarity: a review. Journal of the American Water Resources Association 37, 1085–1101.

23. Douglas, I. 1999. Hydrological investigations of forest disturbance and land cover impacts in South-East Asia: a review. Philosophical Transactions of the Royal Society of London B, 354, 1725-1738.
24. Duvert, C., Gratiot, N., Evrard, O., Navratil, O., Nemery, J., Prat, C., Esteves, M. 2010. Drivers of erosion and suspended sediment transport in three headwater catchments of the Mexican Central Highlands. Geomorphology 123, 243-256.
25. Duvert C., Gratiot, N., Nemery, Burgos, A., Navratil, O. 2001. Sub-daily variability of suspended sediment fluxes in small mountainous catchments – implications for community-based river monitoring. Hydrology and Earth System Science 15, 701-713.
26. FAO. 2013. Aquasta data base, maintained by the Food and Agriculture Organization of the United Nations. Available at http://www.fao.org/nr/water/aquastat/main/index.stm.
27. Fang, N.F., Shi, Z.H., Li, L., Jiang, C. 2011. Rainfall, runoff, and suspended sediment delivery relationships in a small agricultural watershed of the Three Gorges area, China. Geomorphology 135, 158-166.
28. Forsyth, T. Walker, A. 2008. Forest Guardians, Forest Destroyers, the Politics of Environmental Knowledge in Northern Thailand. University of Washington Press: Seattle, WA.
29. Fox, F.M., Vogler, J.B., Sen, O.L., Gambelluca, T.W., Ziegler, A.D. 2012. Simulating land-cover change in Montane Mainland Southeast Asia. Environmental Management 49(5): 968-979.
30. GAME-T. 2013. GAME-T2 Data Center. Available at http://hydro.iis.u-tokyo.ac.jp/GAME-T/GAIN-T/.
31. Gippel, C.J. 1995. Potential of turbidity monitoring for measuring the transport of suspended solids in streams. Hydrological Processes 9, 83–97.
32. Gippel, C.J. 1999. The use of turbidimeters in suspended sediment research. Hydrobiologia 176-177, 465-480.
33. Gray, J.R., Glysson, G.D., Trucios, L.M., Schwarz, G.E. 2000. Comparability of Suspended-Sediment Concentration and Total Suspended Solids Data. Water-Resources Investigations Report 00-4191. U.S. Department of the Interior, USGS.
34. Grayson, R.B., Finlayson, B.L., Gippel, C.J., Hart, B.T. 1996. The potential of field turbidity measurements for the computation of total phosphorus and suspended solids loads. Journal of Environmental Management 47, 257–267.
35. Hartcher, M.G., Post, D.A. 2008. The impact of improved landuse cover on the range of modelled sediment yield from two sub-catchments of the Mae Chaem, Thailand. Mathematics and Computers in Simulation 78, 367-378.
36. Hill, R.D., Peart, M.R. 1998. Land use, runoff, erosion and their control: a review for southern China. Hydrological Processes 12, 2029-2042.
37. Hodgkins R. 1996. Seasonal trend in suspended-sediment transport from an Arctic glacier, and implications for drainage-system structure. Annals of Glaciology 22, 147–151.
38. Hudson, P.F. 2003. Event sequence and sediment exhaustion in the lower Panuco Basin, Mexico. Catena 52, 57-76 .
39. Hurni, H. 1982. Soil erosion in Huai Thung Choa—northern Thailand. Concerns and constraints. Mountain Research and Development 2, 141-156.
40. Janeau, J.L., Bricquet, J.P., Panchon, O., Valentin, C. 2003. Soil crusting and infiltration on steep slopes in northern Thailand. European Journal of Soil Science 54, 543-553.
41. Jansson, M.B. 2002. Determining sediment source areas in a tropical river basin, Costa Rica. Catena 47, 63-84.
42. Jastram, J.D., Zipper, C.E., Zelaznu, L.W., Hyer, K.E. 2010. Increasing Precision of Turbidity-Based Suspended Sediment Concentration and Load Estimates. Journal of Environmental Quality 29, 1306-1316.
43. Kahl, G., Ingwersen, J., Nutniyom, P., Totrakool, S., Pansombat, K., Thavornyutikarn, P., Streck, T., 2008. Loss of pesticides from a litchi orchard to an adjacent stream in northern Thailand. European Journal of Soil Science, 59, 71-81.
44. Kronvang, B., Laubel, A., Grant, R. 1997. Suspended sediment and particulate phosphorus transport and delivery pathways in an arable catchment, Gelbaek Stream, Denmark. Hydrological Processes 11, 627–642.
45. Kummu, M., Varis O. 2007. Sediment-related impacts due to upstream reservoir trapping, the Lower Mekong River. Geomorphology 85: 275-293
46. Landers, M.N., Sturm, T.W., 2013. Hysteresis in suspended sediment to turbidity relations due to changing particle size distributions. Water Resources Research 49, 5487-5500.
47. Langlois, J.L., Johnson, D.W., Mehuys, G.R. 2005. Suspended sediment dynamics associated with snowmelt runoff in a small mountain stream of Lake Tahoe (Nevada). Hydrological Processes 19, 3569-3580.
48. Lawler, D.M., Petts, G.E., Foster, I.D.L., Harper, S. 2006. Turbidity dynamics during spring storm events in an urban headwater river system: The Upper Tame, West Midlands, UK . Science of the Total Environment 360, 109-126.

49. Lefrancois, J., Grimaldi, C., Gascuel-Odoux, C., Gilliet, N. 2007. Suspended sediment and discharge relationships to identify bank degradation as a main sediment source on small agricultural catchments. Hydrological Processes 21, 2923-2933.
50. Legates, D.R., McCabe, G.J. 1999. Evaluating the use of "goodness-of-fit" measures in hydrologic and hydroclimatic model validation. Water Resources Research 35, 233-241.
51. Lenzi, M.A., Marchi, L. 2000. Suspended sediment load during floods in a small stream of the Dolomites (northeastern Italy). Catena 39, 267–282.
52. Lewis, J. 1996. Turbidity-controlled suspended sediment sampling for runoff-event load estimation. Water Resources Research 32, 2299–2310.
53. Lewis, J., Eads, R. 2009. Implementation guide for trubidity threshold sampling: principles, procedures, and analysis. General Technical Report PSW-GTR-212, USDA Forest Service
54. Lim H.S., Boochaphun, K., Ziegler, AD. 2012. Modifiers and Amplifiers of High and low Flows on the Ping River in Northern Thailand (1921-2009): The roles of climatic events and anthropogenic activity. Water Resources Management 26, 4203-4224
55. Lopes, V.L., Ffolliott, P.F. 1993. Sediment rating curves for a clearcut ponderosa pine watershed in northern Arizona. Water Resources Bulletin 29, 369–382.
56. McBean, E.A., Al-Nassri, S. 1988. Uncertainty in suspended sediment transport curves. Journal of Hydraulic Engineering, ASCE 114, 63–74.
57. Meybeck, M., Laroche, L., Durr, H.H., Syvitski, J.P.M. 2003. Global variability of daily total suspended solids and their fluxes in rivers. Global and Planetary Change 39, 65-93.
58. Milliman, J.D., Syvitski, J.P.M. 1992. Geomorphic/tectonic control of sediment discharge to the ocean: The importance of small mountainous rivers. Journal of Geology 100, 525-544.
59. Nash, J.E., Sutcliffe, J.V. 1970. River flow forecasting through conceptual models. Part 1: A discussion of principles. Journal of Hydrology 10, 282–290.
60. Navratil, O., Esteves, M., Legout, C., Nemery, J., Willmore, S., Grangeon, T. 2011. Global uncertainty analysis of suspended sediment monitoring using turbidimeter in a small mountainous river catchment. Journal of Hydrology 398: 246-259.
61. Neef, A., Elstner, P., Chamsai, L., Bollen, A. 2005. Diversity of water management systems: Examples from Hmong and Thai communities in Mae Sa Watershed, Northern Thailand. Mountain Research and Development 25, 20-24.
62. Nelson, B.W. 2001. Sediment dynamics in Rangoon River, Myanmar. Science of the Total Environment 266, 15-21.
63. Nishimura, K., Shimada, T., Yamada, T., Ishikawa, Y., Sukapunnaphan, T. 1997. Hydrological characteristics influenced by deforestation in tropical areas: the Mae Taeng River basin, Thailand. IAHS Publication 245, 125-134.
64. Oeurng, C., Sauvage, S., Sanchez-Perez, J.M. 2010. Dynamics of suspended sediment transport and yield in a large agricultural catchment, southwest France. Earth Surface Processes and Landforms 35, 1289-1301.
65. Old, G.H., Leeks, G.J.L., Packman, J.C., Smith, B.P.G., Lewis, S., Hewitt, E.J., Holmes, M., Young, A. 2003. The impact of a convectional summer rainfall event on river flow and fine sediment transport in a highly urbanised catchment. Science of the Total Environment 314, 495-512.
66. Olive, L.J., Rieger, W.A. 1985. Variation in suspended sediment concentration during storms in small catchments in southeast New South Wales. Australian Geographical Studies 23, 38-51.
67. Ongprasert, S. 1995. Lemon grass (*Cymbopogon citrates*) strips: capacity to control soil erosion and their effect on soil fertility. In: Soil Fertility Conservation Research Report 1994. Mae Jo Univ., Thailand and KU Leuven, Belgium.
68. Orange, D., Pham Dinh Rinh, Toan, T.D., des Tureaux, T.H., Laissus., M., et al. 2012. Long-term measurements on sloping lands in northern Vietnam: impact of land use change on bed load output. Proceedings of the 3rd International Conference on Conservation Agriculture in Southeast Asia, Proceedings. Hanoi Vietnam, December 10-15, 2012. Available at http://horizon.documentation.ird.fr/exl-doc/pleins_textes/divers13-06/010058354.pdf
69. Packman, JJ., Comings, K.J., Booth, D.B. 1999. Using turbidity to determine total suspended solids in urbanizing streams in the Puget Lowlands: in Confronting Uncertainty: Managing Change in Water Resources and the Environment, Canadian Water Resources Association annual meeting, Vancouver, BC, 27–29, October 1999, p. 158–165.
70. Pavanelli, D., Pagliarani, A. 2002. Monitoring water flow, turbidity and suspended sediment load, from an Apennine catchment basin, Italy. Biosystems Engineering 83, 463-468.
71. Picouet, C., Hingray, B., Olivry, J.C. 2001. Empirical and conceptual modeling of the suspended sediment dynamics in a large tropical African river: the Upper Niger river basin. Journal of Hydrology 250, 19-39.

72. Rijsdijk, A., 2012. Surface runoff and sediment yields from tropical volcanic upland watersheds as influenced by climatic, geological, and land-use factors. In: Higgitt, D. (Ed.), Perspectives on Environmental Management and Technology in Asian River Basins. New York, Springer, pp. 69-92.
73. Riley, S.J. 1998. The sediment concentration-turbidity relation: its value in monitoring at Ranger Uranium mine, northern territory, Australia. Catena 32, 1–14.
74. Rodriguez-Blanco, M.L., Taboada-Castro, M.M., Taboada-Castro, M.T. 2010. Factors controlling hydro-sedimentary response during runoff events in a rural catchment in the humid Spanish zone. Catena 82, 206-217.
75. Sadar, M.J. 1998. Turbidity Science, Hach Company. Technical Information Series – Booklet No. 11, Loveland, Colorado.
76. Sammori, T., Yusop, A., Kasran, B., Noguchi, S., Tani, M. 2004. Suspended solids discharge from a small forested basin in the humid tropics. Hydrological Processes 18, 721-738.
77. Sayer, A.M., Walsh, R.P.D., Bidin, K. 2006. Pipeflow suspended sediment dynamics and their contribution to stream sediment budgets in small rainforest catchments, Sabah, Malaysia. Forest Ecology and Management 224, 119-130.
78. Sen, OL, Bozkurt, D., Vogler, J.B., Fox, J.M., Giambelluca, T.W., Ziegler, A.D. 2012. Hydro-climatic effects of future land-cover/land-use change in montane mainland southeast Asia. Climatic Change. DOI 10.1007/s10584-012-0632-0.
79. Sidle, R.C. and Campbell, A.J. 1985. Patterns of suspended sediment transport in a coastal Alaska stream. Water Resources Research 21(6), 909-917.
80. Sidle, R.C., Ziegler, A.D. 2010. Elephant trail runoff and sediment dynamics in northern Thailand. Journal of Environmental Quality 39, 871–881.
81. Sidle, R.C., Ziegler, A.D. 2012. The dilemma of mountain roads. Nature Geoscience 5, 437–438.
82. Sidle, RS, Ziegler, A.D., Negishi, J.N., Abdul Rahim, N., Siew, R. 2006. Erosion processes in steep terrain–truths, myths, and uncertainties related to forest management in SE Asia. Forest Ecology and Management 224, 199-225.
83. Singh, P., Haritashya, U.K., Ramasastri, K.S., Kumar, N. 2005. Diurnal variations in discharge and suspended sediment concentration, including runoff-delaying characteristics, of the Gangotri Glacier in the Garhwal Himalayas. Hydrological Processes 19, 1445-1457.
84. Skarbovik, E., Stalnacke, P., Bogen J., Bonsnes, T.E. 2012. Impact of sampling frequency on mean concentrations and estimated loads of suspended sediment in a Norwegian river: implications for water management. Science of the Total Environment 433, 462-471.
85. Smith, H.G., Dragovich, D. 2009. Interpreting sediment delivery processes using suspended sediment-discharge hysteresis patterns from nested upland catchments, south-eastern Australia. Hydrological Processes 23, 2415-2426.
86. Stubblefield, A.P., Reuter, J.E., Dahlgren, R.A., Goldman, C.R. 2007. Use of turbidometry to characterize suspended sediment and phosphorus fluxes in the Lake Tahoe basin, California, USA. Hydrological Processes 21, 281-291.
87. Takeuchi, K. 1993. Analyses of the flow regime of the Chao Phraya River. IAHS Publication 216, 181-193.
88. Turkelboom, R., Poesen, J., Trebuil, G. 2008. The multiple land degradation effects by land-use intensification in tropical steeplands: a catchment study from northern Thailand. Catena 75, 102-116.
89. Valentin, C., Agus, F., Alamban, R., Boosaner, A., Bricquet, J.P., Chaplot, V., de Guzman, T., de Rouw, A., Januea, J.L., Orange, D., Phachomphonh, K., Do Duy Phai, Podwojewski, P., Ribolzi, O., Silvera, N., Subagyono, K., Thiebaus, J.P., Tran Duc Toan, Vadari, T. 2008. Runoff and sediment losses from 27 catchments in Southeast Asia: impact of rapid land use changes and conservation practices. Agriculture Ecosystems and Environment 128, 225-238.
90. Van Maren, D.S. 2007. Water and sediment dynamics in the Red River mouth and adjacent coastal zone. Journal of Asian Earth Sciences 29, 508-522.
91. Walling, D. E. 1974. Suspended sediment and solute yields from a small catchment prior to urbanisation, in Gregory K.J. and Walling D.E. (Eds), Fluvial processes in instrumented watersheds, Institute of British Geographers ((Special Publication) 6, 169-192.
92. Walling, D.E. 1977. Assessing accuracy of suspended sediment rating curves for a small basin. Water Resources Research 13, 531-538.
93. Walling, D.E. 1999. Linking land use, erosion, and sediment yields. Hydrobiologia 410, 223-240.
94. Walling, D.E. 2006. The sediment load of the Mekong River. Chapter 6.
95. Walling, D.E. 2008. The changing sediment load of the Mekong River. Ambio 37, 150-157.
96. Walling, D. E. and Webb, B. W. 1981. The reliability of suspended sediment load data, in Erosion and sediment transport measurements (Proceedings of the Florence symposium, June 1981), IAHS Publication 133, 177-194.

97. Walling, D.E., Webb, B.W. 1987. Suspended load in gravel-bed rivers: UK experience, in Thorne, C.R., Bathurst, J.C. Hey, R.D. (eds.) Sediment transport in gravel rivers, New York: John Wiley & Sons, pp. 691-723.
98. Wang, J.J., Lu, X.X., 2008. Influence of the changing environment on sediment loads of the Lower Mekong River. IAHS-AISH Publication 325, 612-615.
99. Williams, G.P. 1989. Sediment concentration versus water discharge during single hydrologic events in rivers. Journal of Hydrology 111, 89-106.
100. Williamson, T.N., Crawford, G.G. 2011. Estimation of suspended-sediment concentration from total suspended solids and turbidity data for Kentucky, 1978-1995. Journal of the American Water Resources Association 47, 739-749,
101. Wood, S.H., Ziegler, A.D. 2008. Floodplain sediment from recent 50-year-recurrence floods of the Ping River in northern Thailand. Hydrology and Earth Systems Science 12, 959-973.
102. Xu, K.H, Milliman, J.D. 2009. Seasonal variations of sediment discharge from the Yangtze River before and after impoundment of the Three Gorges Dam. Geomorphology 104, 276-283.
103. Ziegler, A.D., Lu, X.X., Tantasarin, C. 2011. Sediment load monitoring in the Mae Sa catchment in northern Thailand. Sediment Problems and Sediment Management in Asian River Basins (Proceedings of the Workshop held at Hyderabad, India, September 2009). IAHS Publication 349, 86-91.
104. Ziegler, AD, Giambelluca, T.W. 1997. Importance of rural roads as source areas for runoff in mountainous areas of northern Thailand. Journal of Hydrology 196, 204-229.
105. Ziegler, A.D., Sutherland, R.A., Giambelluca, T.W. 2001a. Acceleration of Horton overland flow and erosion by footpaths in an agricultural watershed in Northern Thailand. Geomorphology 41: 249-262.
106. Ziegler, A.D., Giambelluca, T.W., Sutherland, R.A., Vana, T.T., Nullet, M.A. 2001b. Contribution of Horton overland flow contribution to runoff on unpaved mountain roads in northern Thailand. Hydrological Processes 15, 3203-3208.
107. Ziegler, A.D., Giambelluca, T.W., Nullet, M.A., Sutherland, R.A., Tantasarin, C., Vogler, J.B., Negishi, J.N. 2009a. Throughfall in an evergreen-dominated forest stand in northern Thailand: comparison of mobile and stationary methods. Agriculture and Forest Meteorology 149, 373 – 384.
108. Ziegler, A.D., Bruun, T.B., Guardiola-Claramonte, M., Giambelluca, T.W., Lawrence, D., Nguyen Thanh Lam. 2009b. Environmental consequences of the demise in swidden agriculture in SE Asia, Hydrology and geomorphology. Human Ecology 37, 361-373.
109. Ziegler, A.D., Giambelluca, T.W., Sutherland, R.A., Nullet, M.A., Yarnasarn, S., Pinthong, J., Preechapanya, P., Jaiaree, S. 2004. Toward understanding the cumulative impacts of roads in agricultural watersheds of Montane Mainland Southeast Asia. Agriculture Ecosystems and Environment 104, 145–158
110. Ziegler, A.D., Negishi, J.N. Sidle, R.C. Preechapanya, P., Sutherland, R.A., Giambelluca, T.W., Jaiaree, S. 2006. Reduction of stream suspended sediment concentration by a riparian buffer: filtering of road runoff. Journal of Environmental Quality 35, 151-162.
111. Ziegler, A.D., Petney, T.N., Grundy-Warr, C., Andrews, R.H., Baird, I., Wasson, R.J., Sithithaworn, P., 2013. Dams and disease triggers on the Mekong River. PLoS Neglected Tropical Diseases, 7, 1-4.

FIGURE CAPTIONS

Fig. 1 (a) Location of Mae Sa study area in northern Thailand in relationship to other major rivers. (b) Major land covers in the Mae Sa catchment include hill slope and plantation agriculture (AG, 23%), greenhouse agriculture (GH, 7%), urbanized or peri-urban areas (U, 8%), and forest of various degrees of disturbance (F, 62%). Grid cell dimensions are 2x2 km. Dark rectangles demarcate hydro-meteorological measurement sites; and gray rectangles are the station elevations. Streamflow variables were monitored at location 434. Rainfall is measured at all other numbered stations (rectangles).

Figure 2. (A) Mean annual rainfall (2006-2008) for the 11 stations spanning an elevation range of 540 to 1240m (figure 1). Error bars are standard errors. The low value at 910 m appears to be in a rain shadow (Station 427). (B) Discharge (Q) rating curve for station 434 on the Mae Sa River (h is river stage). The modified equation was determined following a noticeable change in the stream channel bed on 27 July 2006.

Figure 3. (A) ADZ measuring high concentrations in Mae Sa River during a pilot study in 2005; (B) Kalaya filtering the sediment for determination of <63 μm fraction; (C) wet sieving the > 2000 μm and 63-1000μm TSS fractions; (D) SGB installing the turbidity probe inside PVC pipe cantilever.

Figure 4. Spatial distribution of rainfall for all 18 monitored events. Numbers correspond to year, month, and day. Rainfall was measured at 11 locations (see Figure 1). For many storms the spatial distribution of rainfall is highly variable over the 74-km^2 catchment.

Figure 5. Relationship between measured discharge and total suspended solids (TSS) during 18 events. Clockwise, anti-clockwise, and complex types of hysteresis were observed, as were cases of uncertain or no clear pattern in hysteresis. Rising and falling limb refer to the discharge hydrograph (not shown).

Figure 6. Reasonably strong predictive relationship (R^2 = 0.87) between turbidity (T) and total suspended solid concentrations (TSS) over a narrow range of T values (5-2800 NTU), and corresponding TSS values (27-8355 mg l^{-1}).

Figure 7. Comparison of total suspended solids (TSS), turbidity, and discharge for data collected in 2006 (n=125), 2007 (n=107), 2008 (n=101). The entire 333 value data set is combined in panels d, h, and l.

Figure 8. Observed turbidity versus total suspended solids (TSS) for three size fractions for 2006 (circles) and 2007 (crosses).

Figure 9. Observed versus estimated total suspended solids (TSS), determined by several equations during the development of the annual time series. See text for descriptions of all equations. Annual total suspended solid loads for years 2006-2008 in Figure 10 were estimated using equation 10.

Figure 10. Hourly and cumulative discharge (Q), turbidity (NTU) and total suspended solids (TSS) for the three year study period. In all panels, the thick line is the estimated cumulative total suspended solid load (Mg); and the dotted line represents the error in the estimate (Table 4).

Figure 11. (a) Mean (or median) sediment yields for various northern Thailand Rivers (Table 1) plotted against mean annual discharge rate; (b) Maximum reported sediment yields plotted against catchment area. The data are partitioned into those considered reliable and those for which we were uncertain of their reliability (see footnote in Table 1). The Mae Sa river investigated in this study is indicated by a square.

Figure 12. Yearly changes in the relationship between discharge and total suspended solids (calculated as the mean hourly value for each month) demonstrate a general clockwise hysteresis pattern for all years – which is particularly noticeable in the late wet-season months (July – Nov). Complicating the pattern are early season flushes from large storms prior to the typical onset of the wet season (e.g., March and May, 2007), as well as in/near channel construction in January of 2007 (hence the high initial value).

Figure 13. Estimated (thin line) versus measured (circles) total suspended solid concentrations (TSS) for 18 events. Calculations are based on Equation 5 using the parameters listed in Table 5. The thick lines are the estimated cumulative event total suspended solids (TSS) loads, which are listed in Table 3.

Figure 14. For three sample events, differences in (a) the relationship between turbidity and total suspended solids (TSS); (b) particle size distribution; and (c) the discharge-turbidity hysteresis effect. All samples were taken during periods of high turbidity (E1 and E2 are from different sediment peaks of the same storm). The particle size distributions of sediment at each sampling time are greatly different, as is the relationship between measured turbidity and TSS. The differences demonstrate how separate regression equations based on the sediment sources would be better than one common equation. Note: these data are for events sample during a pilot study in 2005, for which we used a turbidity probe that could register values up to 4000 NTU.

Figure 15. Observed versus estimated total suspended solids for three size fractions for six storms in each of 2006 and 2007. Fractions were predicted with storm-specific variations of Equation 5 (not shown). For the 12 storms, material <63 μm in diameter comprised on average about 67% of the TSS in the 98 samples. Approximately 32% was material in the 63-2000 μm diameter class; and 1% was material greater than 2000 μm.

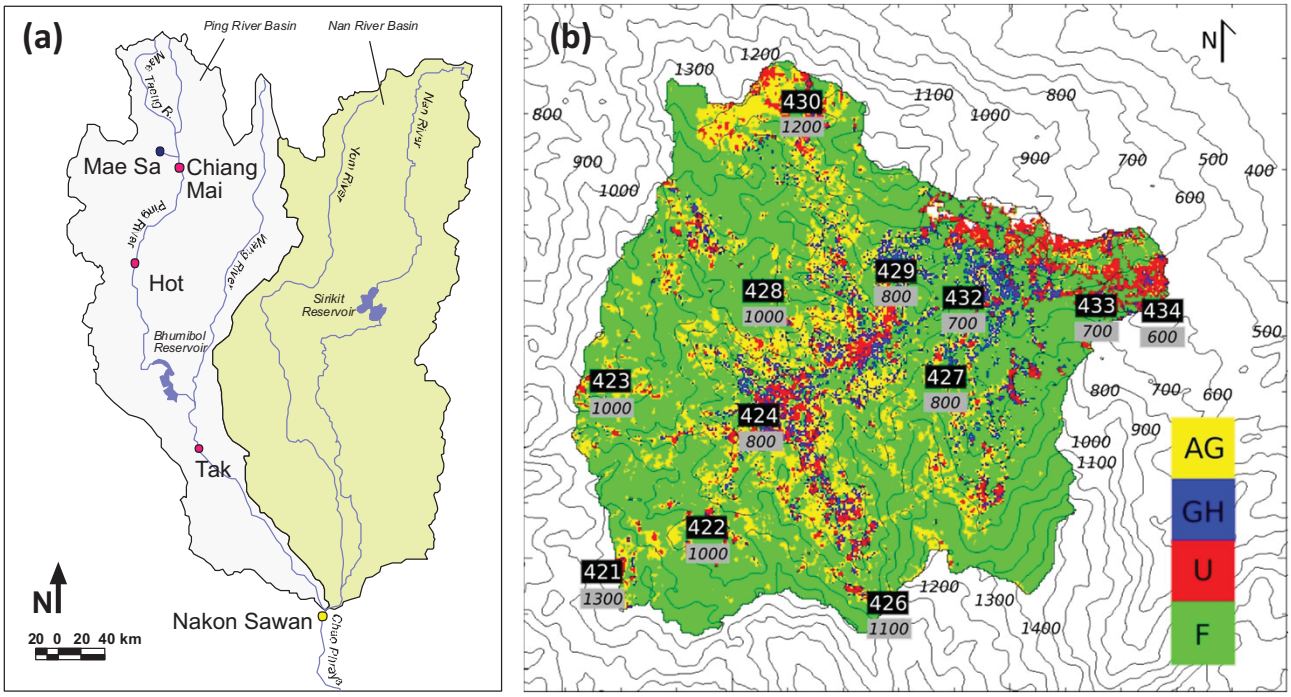

Figure 1

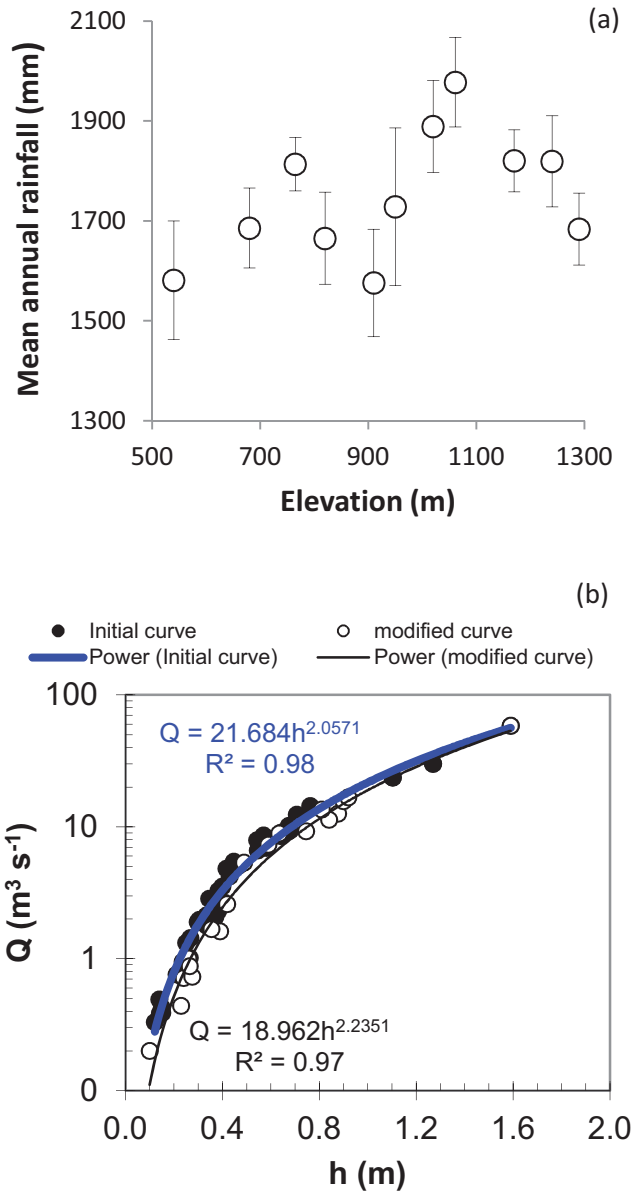

Figure

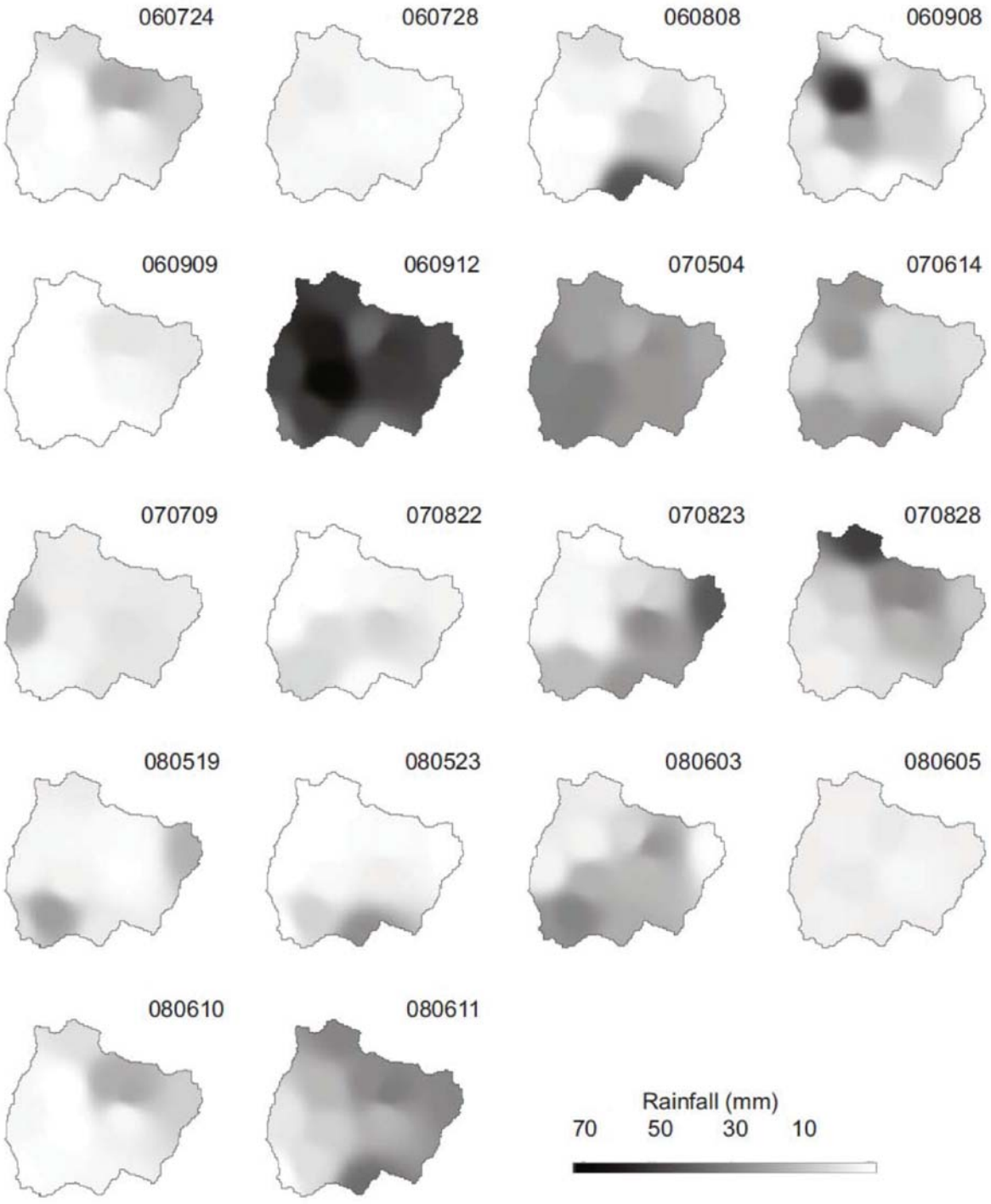

Figure

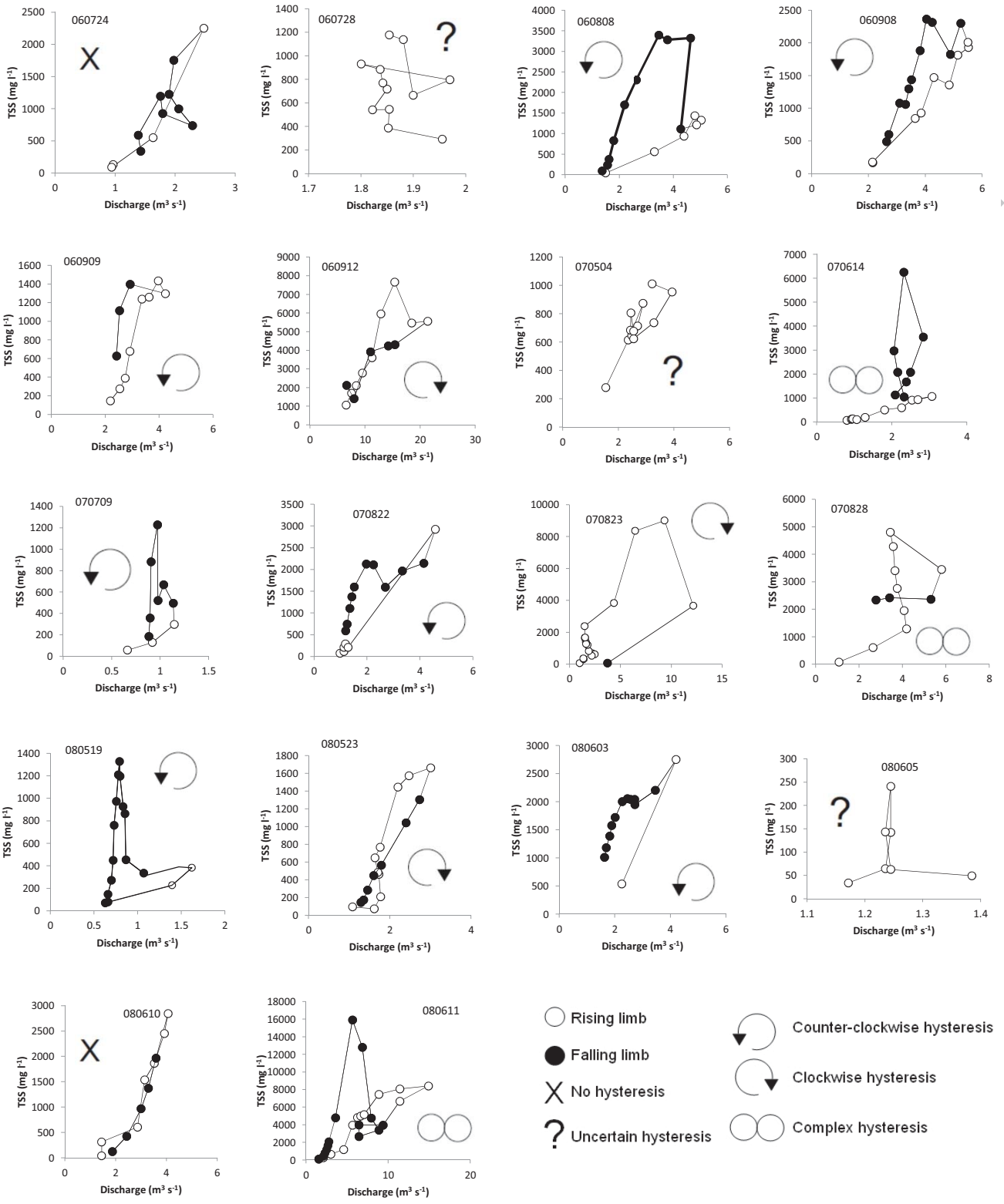

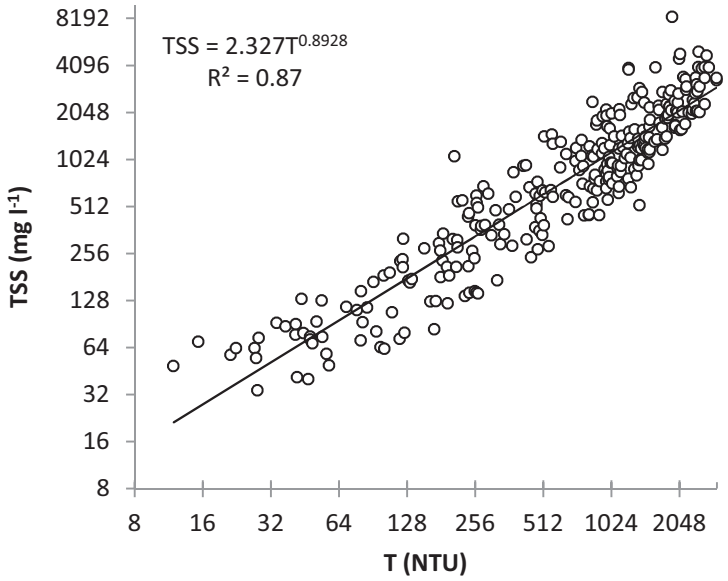

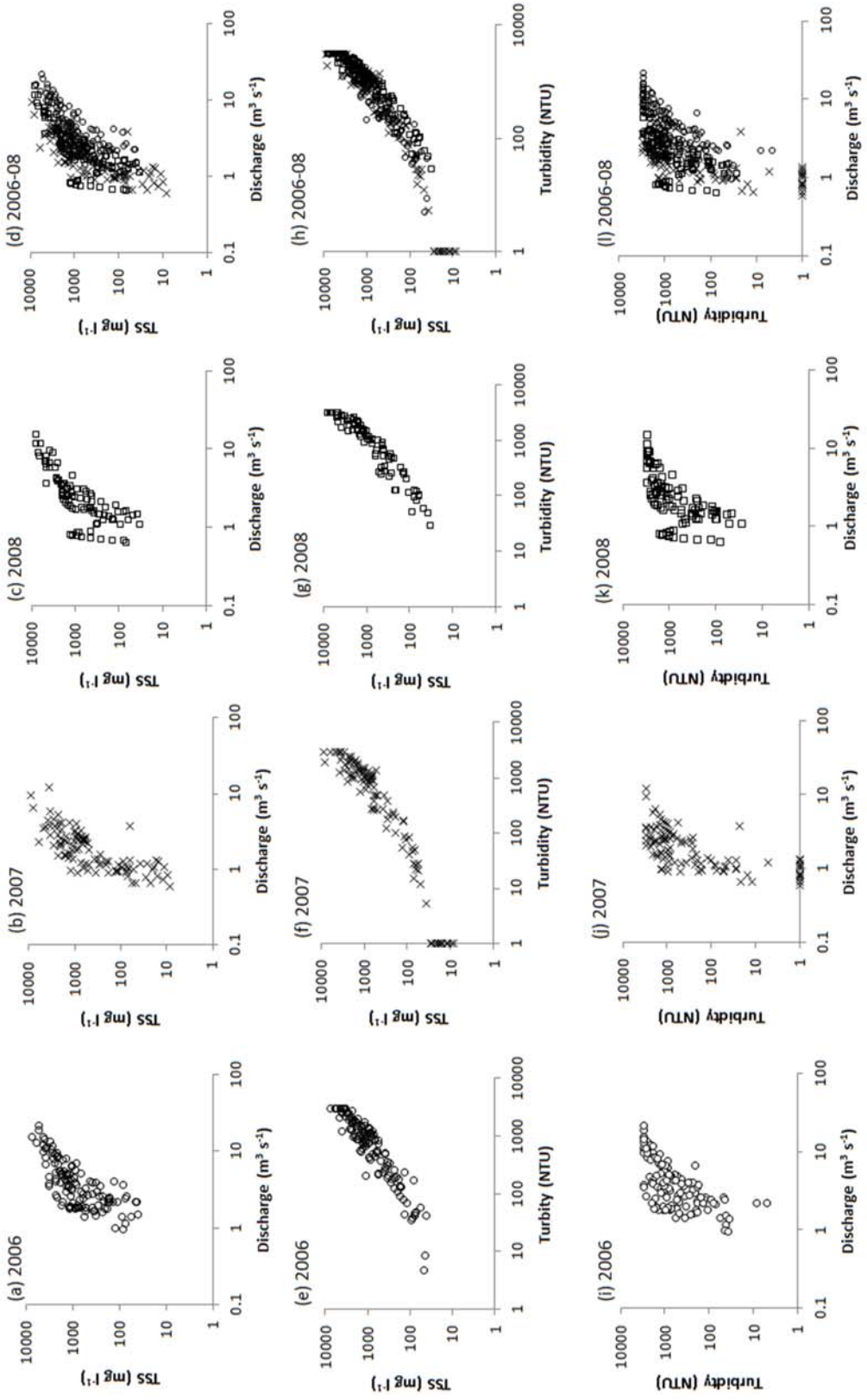

Figure

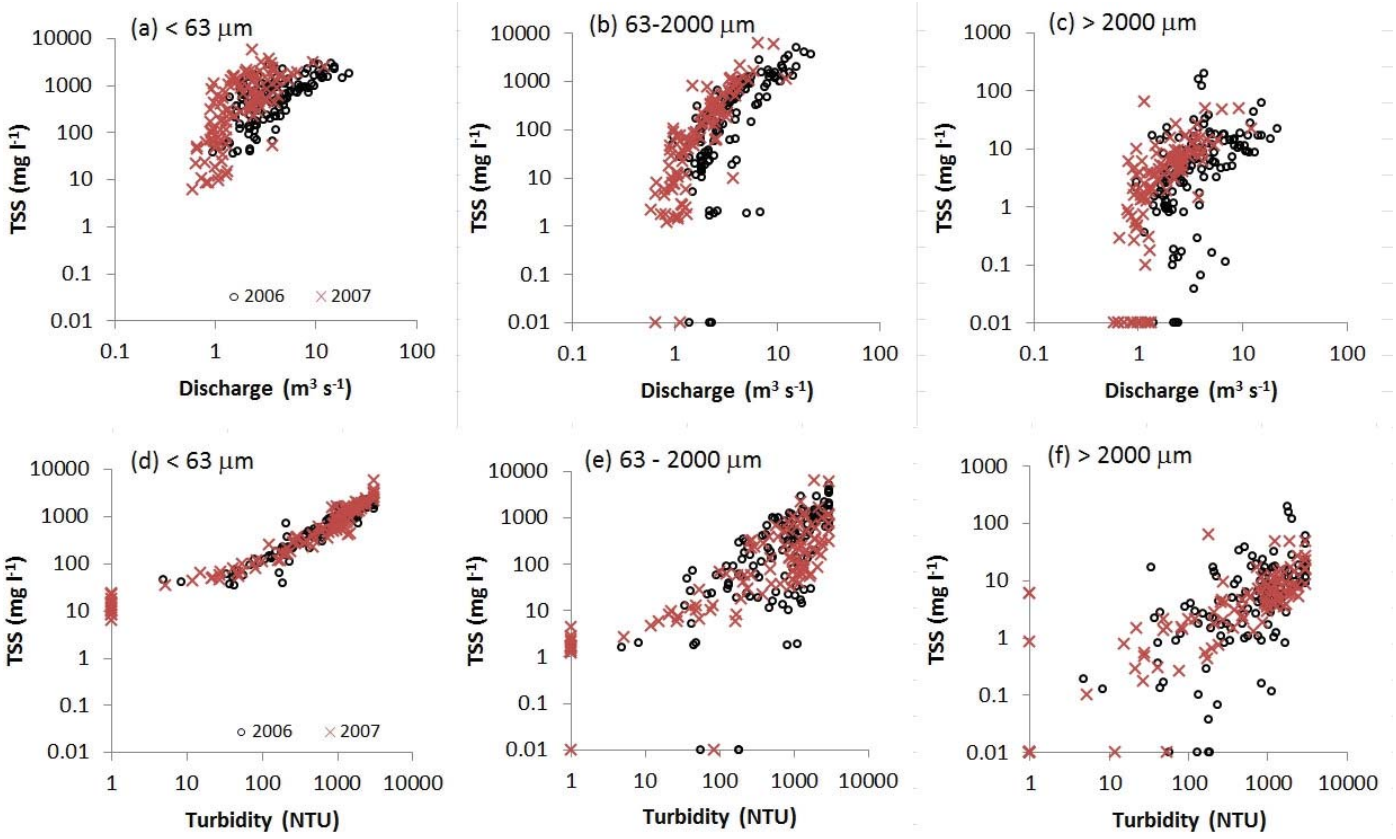

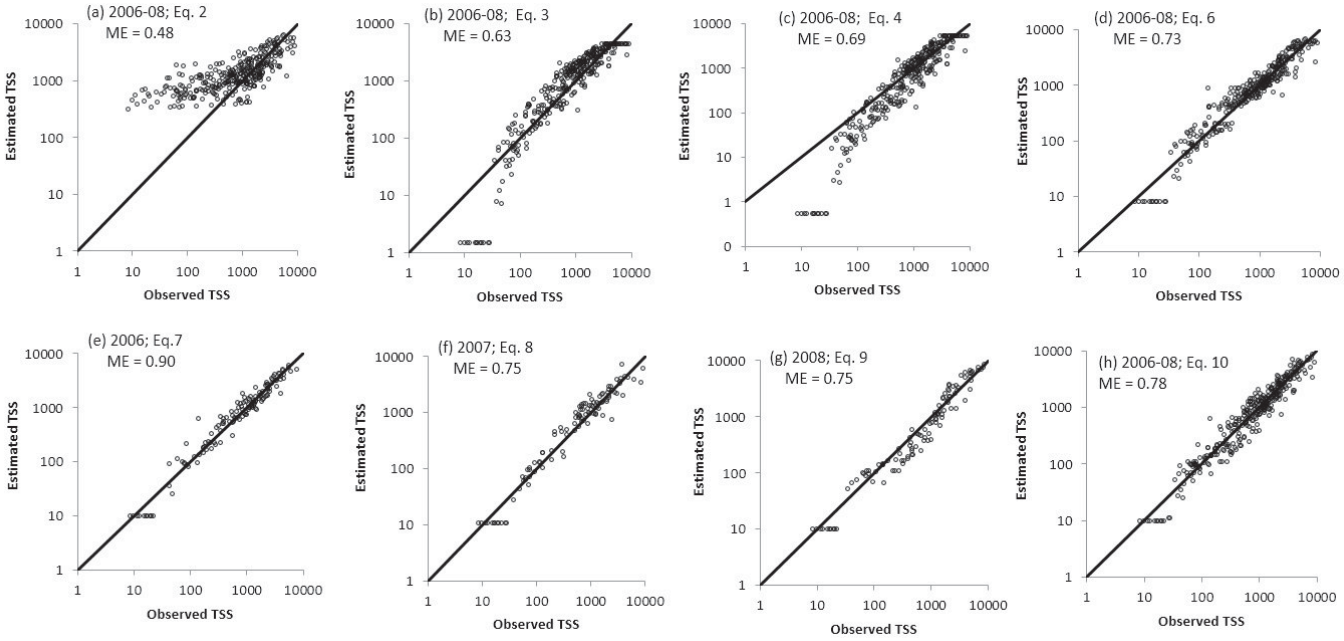

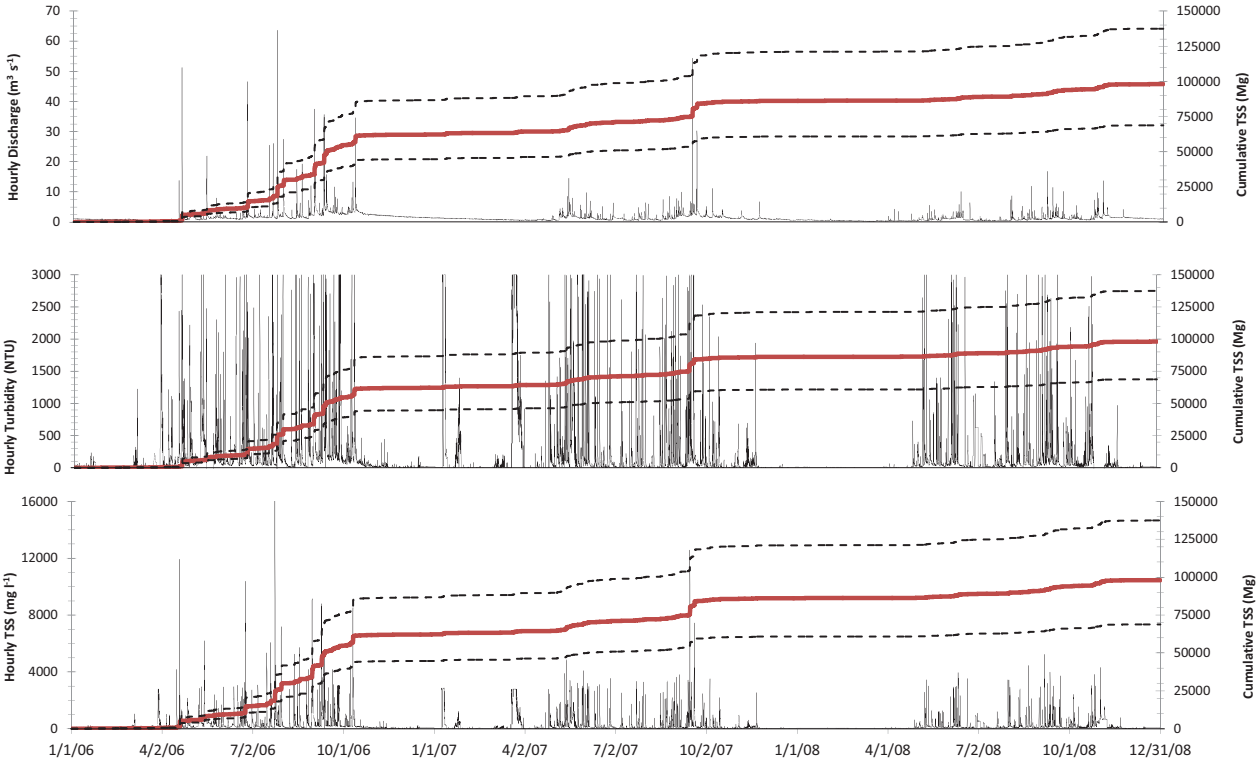

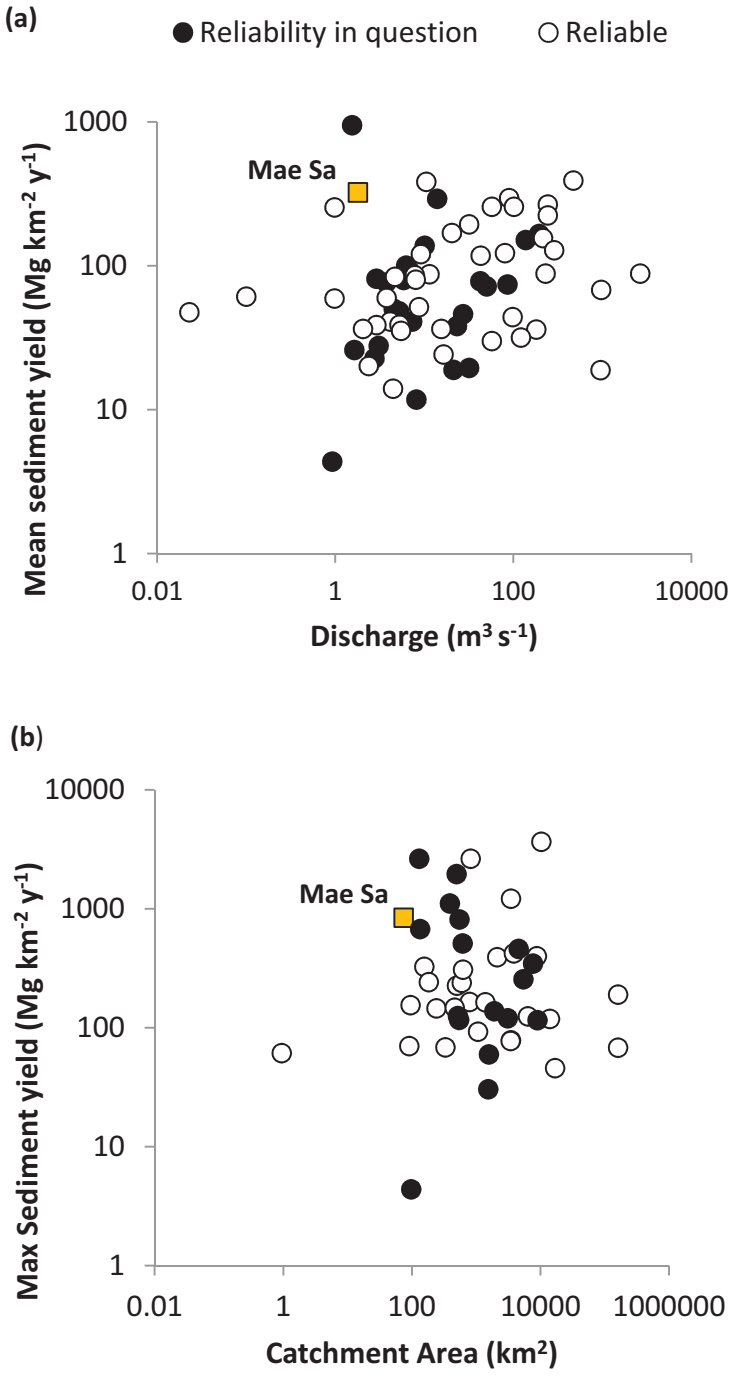

Figure

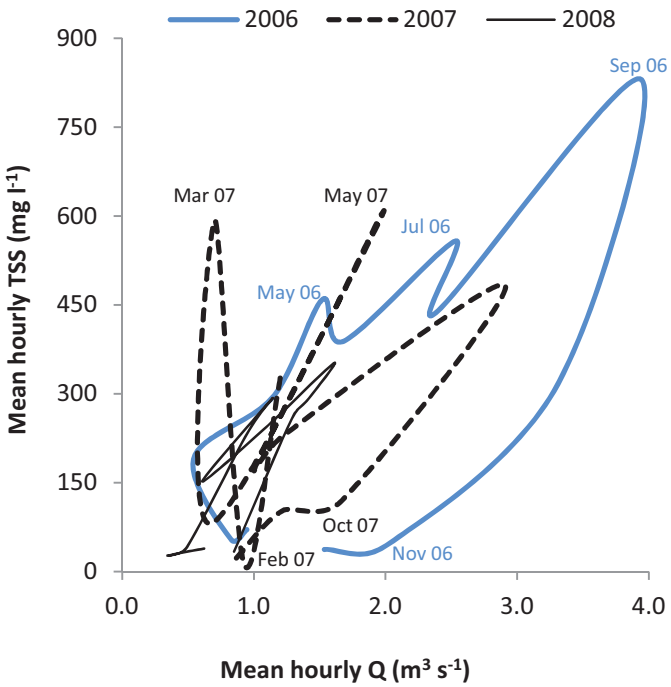

Figure

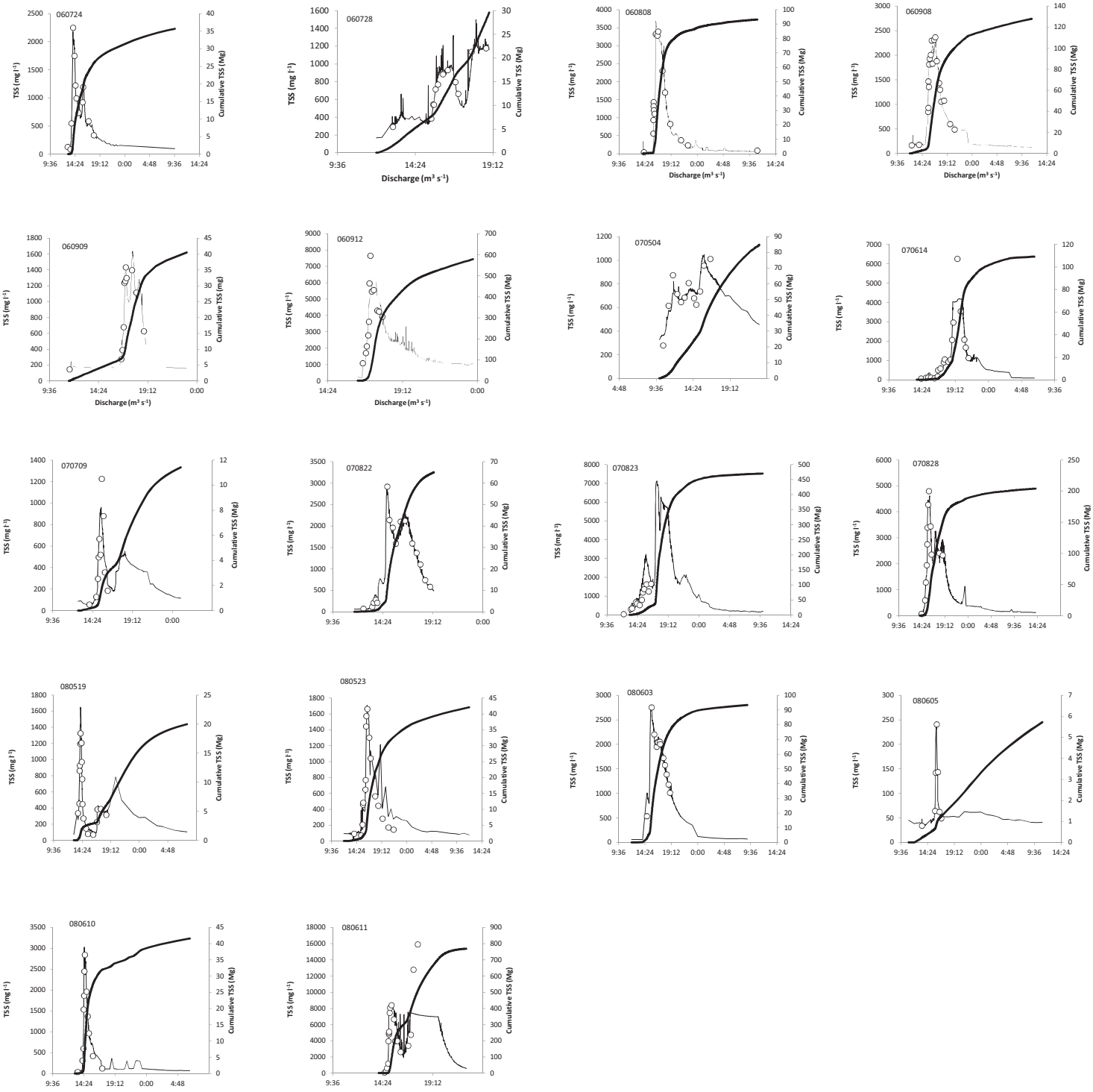

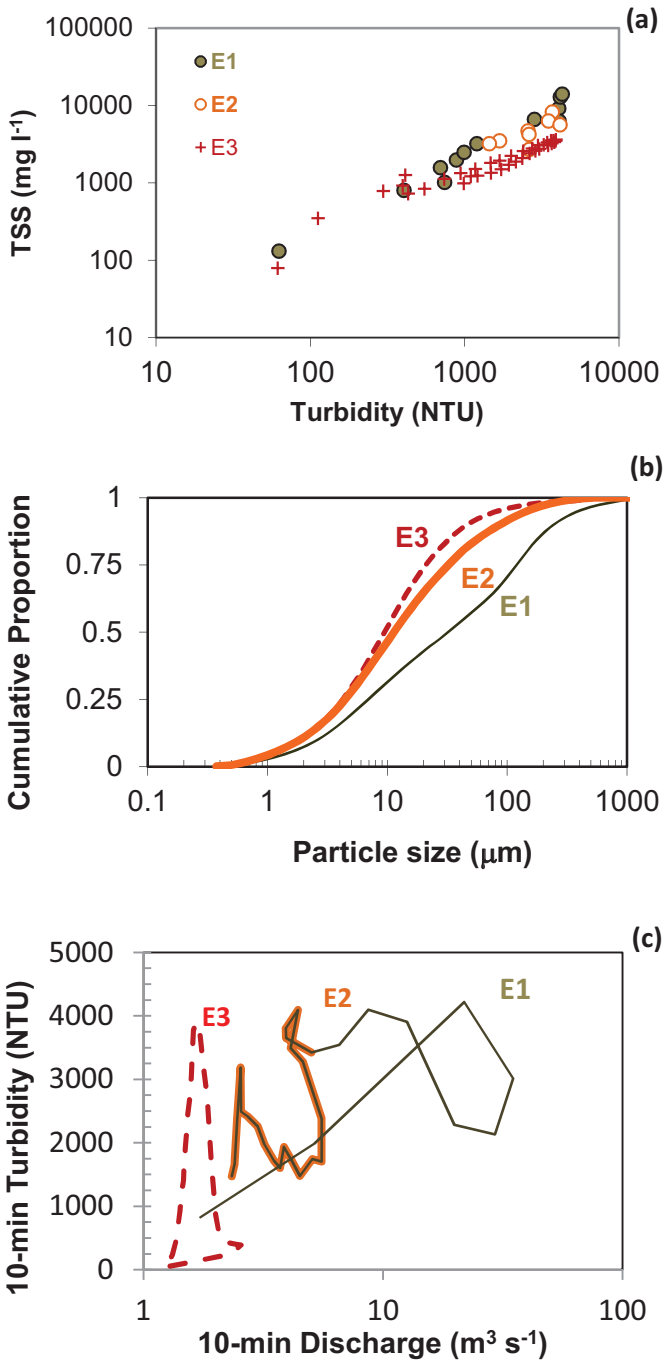

060724

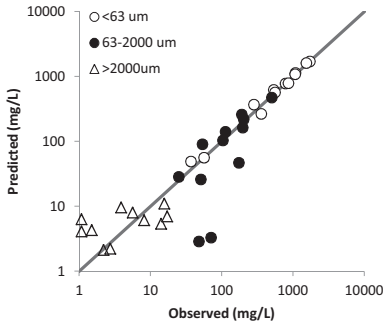

060728

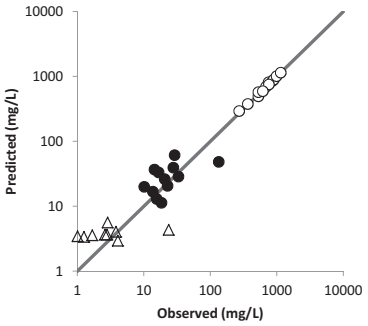

06808

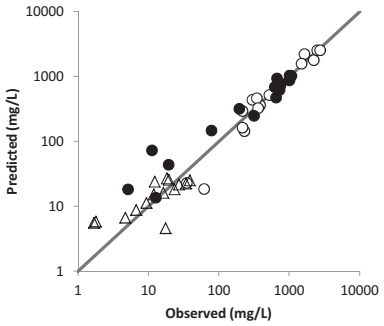

060908

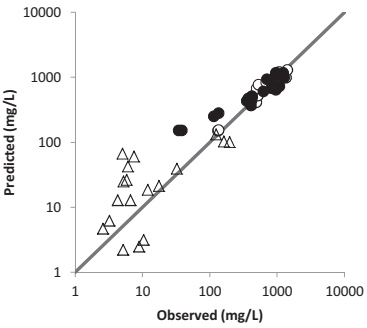

06909

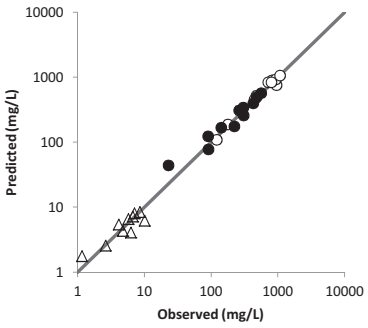

060912

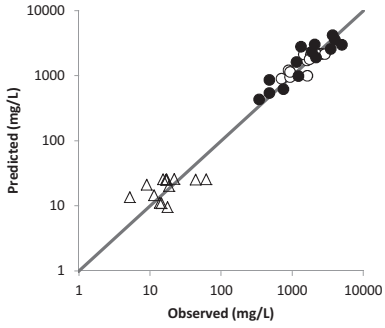

070504

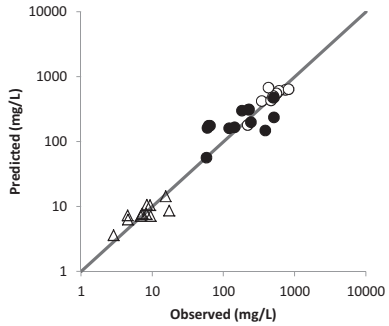

070614

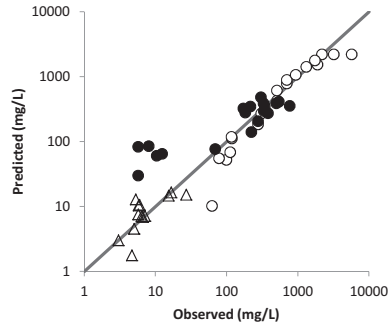

070709

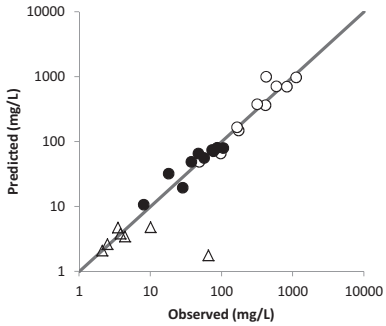

070822

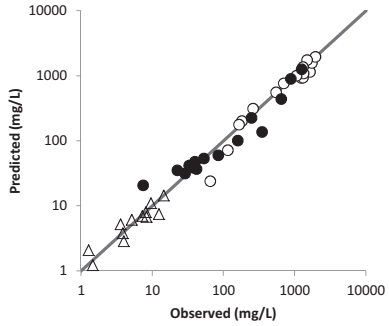

070823

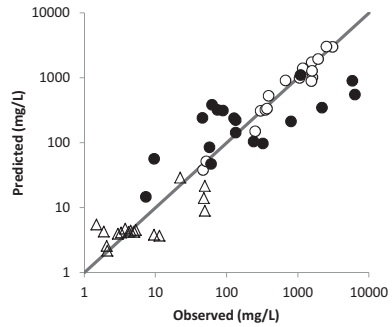

070828

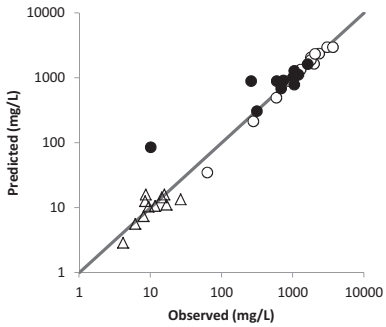

Table 1. Annual mean discharge, annual catchment sediment yield, and annual sediment concentrations for various rivers in northern Thailand.

River/stream	Area	Q_{annual}	$Yield_{annual}$	Con_{mean}	Period	Reference
	km^{-2}	m^3s^{-1}	$Mg\ km^{-2}y^{-1}$	$mg\ l^{-1}$		
Reliable						
Nan (Tha Pla)	12790	470	391	337	55-63	FAO (2013)
Nam Pat (N33, Ban Wang Bang, Nan)	2463	10	383	2862	81-87	FAO (2013); GAME-T (2013)
Mae Sa (Mae Rim, Chiang Mai)	74.16	2	323	422	06-08	This study
Nan (N64, Tha Wang Pha, Nan)	3476	90	294	4	07-11	RID (2012)
Nan (N23; Ban Phra Fang)	16336	244	266	566	80-81	FAO (2013); GAME-T (2013)
Nam Wa (N42, Lai Nan, Wiang Sa, Nan)	2107	57	257	301	97-02	RID (2012)
Nan (N1, Nan)	4609	101	256	370	52-88	Alford (1992)
Nan (N13A, Wiang Sa, Nan)	8784	243	223	256	94-2007	RID (2012)
Chaem (P14, Hang Dong, Chiang Mai)	3853	32	194	743	68-76, 83-93; 00-05	RID (2012)
Taeng (Station 7; Mae Taeng)	1900	20	168	498	75-93	Nishimura et al (1997)
Nan (N.5A; Muang, Nam)	25294	215	156	579	80-99	FAO (2013); GAME-T (2013)
Huai Mee (Phrae)	0.118	0	128	104	03	Bricquet et al. (nd)
Nan (N5A; Muang)	25491	287	128	361	81-99	FAO (2013); GAME-T (2013)
Suk (Mae Chaem)	95	1	254	785	95,03 (sims)	Hartcher and Post (2008)
Yom (Y37, Wang Chin, Phrae)	10306	80	122	5	07-11	RID (2012)
Nam Yao (N49, Pua, Nan)	155	9	120	65	00-05	RID (2012)
Yom (Y20, Song, Phrae)	5410	43	117	467	52-88	Alford (1992)
Kong (Mekong; at Chiang Saen)	391,000	2653	88	412	93-00	Lu and Siew (2005)
Ping (Wang Kra Chao)	26386	230	88	320	52-53	FAO (2013)
Nam Khuan (Y36, Pong, Phayao)	822	11	87	199	00-05	RID (2012)
Tuen (P64, Om Koi, Chiang Mai)	503	8	86	177	97-00	RID (2012)
Pai (Ban Na Chalong)	369	5	84	209	96-97	Meybeck et al (2003)
Wang (W16, Lamphang)	1284	8	80	407	52-88	Alford (1992)
Huai Ma (Phrae)	0.096	0	79	74	03	Bricquet et al. (nd)
Chao Phraya	160,000	964	68	324	NR	Takeuchi (1993); Milliman and Syvitski (1992)
Huai Khun Loei (Pa Pae, Chiang Mai)	1	0	61	18	00	Ziegler et al. (2000)
Nam Haeng (N63, Na Noi, Nan)	788	4	60	395	97-05	RID (2012)
Kong Kha (Mae Chaem)	91	1	59	172	95,03 (sims)	Hartcher and Post (2008)
Wang (W16A, Chae Hom, Lamphang)	1388	9	52	262	00-11	RID (2012)
Huai Ma Nai (Phrae)	0.932	0	47	61	03	Bricquet et al. (nd)
Ping (P19A, Ban Tha Sala, Chom Thong)	14,023	98	44	200	52-88	Alford (1992)
Nam Pi (Y24, Chiang Muan, Phayao)	597	4	41	188	97-05	RID (2012)
Soi (W17, Chae Hom, Lamphang)	619	5	39	145	96-11	RID (2012)
Taeng (P65, Wiang Haeng, Chiang Mai)	240	3	39	102	93-00	RID (2012)
Wang (W1C, Lamphang, Lamphang)	3478	16	36	258	94-96; 07-08; 10-11	RID (2012)
Taeng River (P70, Wiang Haeng, Chiang Mai)	182	2	36	103	95-97;99-00	RID (2012)
Ping (Kampang Petch)	42300	180	36	268	51-57	FAO (2013)
Klang (P24a, Cham Thong, Chiang Mai)	460	5	35	94	97-01	RID (2012)
Ping (P73, Cham Thong, Chiang Mai)	16815	122	32	139	01-07	RID (2012)
Ping (P1, Nawarat Bridge, Chiang Mai).	6355	57	30	106	93-11	RID (2012)
Wang (W21, Lamphang, Lamphang)	3415	16	24	159	99-11	RID (2012)
Huai Tong (Phrae)	0.071	0	22	28	03	Bricquet et al. (nd)
Lai (Y34, Phrae, Phrae)	331	2	20	89	97-02	RID (2012)
Chao Phraya	160,000	951	19	139	NR	Milliman et al., (2011)
Dui (W20, Lamphang, Lamphang)	1065	4	14	106	96-03; 05	RID (2012)
Reliability uncertain						
Lai (P80, Doi Saket, Chiang Mai)	129	2	947	2515	06-11	RID (2012)
Taeng (P13; Kaeng Kut*)	1747	14	292	1160	80	FAO (2013); GAME-T (2013)
Taeng River (P4A, Mae Taeng, Chiang Mai)	1902	10	137	823	92-05; 07-12	RID (2012)
Yom (Kaeng Luang)	12658	194	166	343	81-99	FAO (2013)
Wang (W.4A; Ban Wang Man)	10507	138	151	365	81-99	FAO (2013); GAME-T (2013)
Nam Mae Tun (p64; Ban Mae Tun)	503	6	100	255	92-94	FAO (2013); GAME-T (2013)
Kuang (P34; Ban Pha Taek)	566	7	93	247	81	FAO (2013); GAME-T (2013)
Huai Nam Yao (N65, Tha Wang Pha, Nan)	615	3	81	547	97-05; 07-10	RID (2012)
Wang (P82, Mae Wang, Chiang Mai)	389	6	80	167	06-11	RID (2012)
Yom (Y20, Song, Phrae)	5410	42	78	315	75-93; 06-11	RID (2012)
Wang (P84; Thung Pi, Wang, Chiang Mai)	493	4	76	319	06-11	RID (2012)
Nan (N1, Muang, Nan)	4560	85	74	125	78-93; 06-11	RID (2012)
Yom (Y1C, Phrae, Phrae)	7624	50	72	346	97-11	RID (2012)
Rim (P21, Mae Rim, Chiang Mai)	515	5	50	182	01-11	RID (2012)
Ngat (P56A, Phrao, Chiang Mai)	539	5	48	158	00-11	RID (2012)
Nam Khek (N24; Ban Wang Nok)	1861	27	46	100	80-99	FAO (2013); GAME-T (2013)
Nam Pua (N50; Bridge)	192	7	41	34	82-97	FAO (2013); GAME-T (2013)
Ping (P75, Mae Taeng, Chiang Mai)	3090	23	38	162	01-11	RID (2012)
Nam Haeng (N63; bridge)	788	3	28	227	87-99	FAO (2013); GAME-T (2013)
Kuang (P79, Doi Saket, Chiang Mai)	134	2	26	68	06-11	RID (2012)
Tha (P77, Mae Tha, Lamphun)	547	3	23	143	00-10	RID (2012)
Wang (W3A, Thoen, Lamphang)	8985	32	20	174	97-03,05,07-11	RID (2012)
Kuang River (P5, Muang, Lamphun)	1569	21	19	44	07-12	RID (2012)
Li (P76, Li, Lamphun)	1541	8	12	71	01-05; 07-10	RID (2012)
On (P86, San Kamphaeng, Chiang Mai)	97	1	4	15	07	RID (2012)

RID TSS values were calculated as medians of years indicated in the period column; corresponding Q values are also medians, but the range of years is usually longer (not shown). The data for which the reliability is uncertain are of two types: (i) values that were originally reported in units of 100t/year, and represented improbably high yields for some rivers. Thus we assumed the units should have been t/year for all rivers with these units. (ii) values that were calculated from two different datasets with limited entries (FAO (2013), RID (2012); GAME-T (2013)). Sim refers to a simulation period. Annual sediment concentration is calculated as the annual sediment load divided by the annual runoff (neither value is shown).

Table 2. Rainfall depth for eleven stations (#421-433) for 18 storms in Mae Sa Catchment

Event/date	421	422	423	424	425	427	428	429	430	432	433	Basin RF	Duration	I_{60_max}
	(mm)	(mm)	(mm)	(mm)	(mm)	(mm)	(mm)	(mm)	(mm)	(mm)	(mm)	(mm)	(h)	(mm h^{-1})
060724	0.0	1.4	0.0	1.4	3.8	9.4	1.0	2.4	0.5	3.2	2.2	2.5	1.9	5.5
060728	2.5	3.0	4.7	2.3	4.4	0.3	5.8	2.7	1.8	2.6	1.1	2.9	2.5	3.7
060808	1.2	1.4	0.0	0.0	43.3	13.5	3.5	2.2	8.1	7.9	2.4	8.0	11.0	42.8
060908	6.7	3.6	5.3	24.5	0.3	12.4	52.7	7.3	0.5	13.5	1.1	13.5	9.0	42.7
060909	0.0	0.0	0.0	0.0	0.0	2.8	0.5	7.4	0.3	7.6	6.9	2.4	9.0	7.6
060912	33.5	49.3	47.3	65.1	34.7	49.0	56.9	38.7	47.5	50.5	44.9	48.1	22.0	28.8
070504	28.4	32.6	28.4	32.6	36.7	23.9	29.1	20.9	29.1	24.3	17.0	27.1	10.9	16.9
070614	24.9	24.9	9.7	13.9	28.6	10.4	27.1	9.6	27.1	10.7	8.2	17.3	4.3	21.4
070709	2.5	2.5	18.5	4.6	7.4	8.4	5.3	5.7	5.3	6.5	6.0	6.9	2.2	17.3
070822	10.9	10.9	0.6	9.7	1.4	11.6	0.3	2.2	0.0	4.0	3.8	4.5	1.5	9.4
070823	17.5	17.5	1.9	2.3	27.2	30.2	2.9	7.7	0.5	11.7	42.4	16.5	5.0	38.1
070828	4.7	4.7	6.3	9.2	8.7	18.6	13.6	30.5	48.5	31.0	13.2	16.0	3.5	29.5
080519	8.8	24.9	3.1	4.0	5.7	1.0	2.6	1.9	5.5	1.6	20.0	7.8	2.9	19.2
080523	0.0	11.8	0.0	2.6	28.9	5.2	0.3	1.6	0.3	1.6	0.5	5.1	1.5	27.8
080603	27.6	31.5	3.7	20.0	21.3	18.3	3.9	10.4	5.1	26.3	0.8	13.0	4.6	27.4
080605	5.3	4.4	5.4	6.4	5.4	2.8	4.5	6.5	4.8	4.5	4.9	4.9	3.9	5.7
080610	0.0	1.7	3.1	0.3	2.7	2.6	0.3	20.9	9.1	22.5	12.8	6.5	1.5	21.9
080611	1.2	9.2	6.9	12.6	36.7	18.9	18.6	29.7	31.1	33.2	30.9	21.9	2.3	35.4
Weights	0.028	0.087	0.093	0.091	0.102	0.102	0.143	0.079	0.066	0.053	0.156	1	-	-
Elevation (m)	1290	1020	1170	765	1061	910	950	820	1240	680	540	-	-	-

Event/date reflects year, month, day. Rainfall station locations are shown in figure 1. Weights are used in the calculation of catchment –wide rainfall via the Theissen method; and $I_{60\text{-}Max}$ is the maximum 60-minute rainfall intensity during the event.

Table 3. Discharge (Q) and total suspended solid (TSS) variables for 18 storm events in Mae Sa River, 2006-2008.

Event/date	n_{TSS}	Q_I	Q_P	Q_T	ROC	Duration	n_T	T_{max}	TSS_{max}	TSS_{load}	$TSS_{<63\mu m}$	$TSS_{<63-2000\mu m}$	$TSS_{>2000\mu m}$
		$m^3 s^{-1}$	$m^3 s^{-1}$	m^3	-	H	-	NTU	$g m^{-3}$	Mg	%	%	%
060724	12	1.0	2.5	89665	0.49	20.6	330	1680	2252	36	86	13	1
060728	12	2.0	2.1	47325	0.22	7	318	1728	1177	30	95	4	1
060808	11	1.6	6.0	112732	0.19	21.1	1264	3000	3279	92	74	25	1
060908	16	2.3	6.6	221097	0.22	23.5	534	2023	2365	128	53	45	2
060909	20	2.4	4.9	96307	0.53	11.5	323	1247	1434	41	71	28	1
060912	14	8.0	29.7	224898	0.06	7.4	316	3000	7658	579	49	50	1
070504	14	1.6	4.6	120458	0.06	13	501	1496	954	85	69	30	1
070614	19	0.8	3.5	100483	0.08	18.8	512	3000	6251	110	76	23	1
070709	10	0.6	1.2	37930	0.07	12.3	295	1369	1226	11	84	15	1
070822	16	1.0	5.4	48666	0.15	7.6	392	2347	2920	65	78	22	0
070823	18	1.0	15.9	181914	0.15	20.9	479	3000	9001	469	78	21	1
070828	12	1.1	7.0	167113	0.14	24	528	3000	4802	204	61	39	0
080519	19	1.1	1.7	63427	0.11	19	311	1594	1327	20	NA	NA	NA
080523	17	1.1	3.4	111459	0.30	24	214	1417	1661	42	NA	NA	NA
080603	13	2.5	4.9	116524	0.12	21	395	2523	2204	93	NA	NA	NA
080605	7	1.1	1.4	111873	0.31	24	189	454	241	6	NA	NA	NA
080610	12	1.5	4.7	116459	0.24	17.7	206	2356	2845	42	NA	NA	NA
080611	16	1.6	19.9	260336	0.16	26	702	3000	15906	788	NA	NA	NA

Event/date reflects year, month, day; n is the number of manually collected total suspended solid concentration and discharge samples obtained during an event; Q_I is initial discharge; Q_P is peak discharge; Q_T is total event stormflow; ROC is event runoff coefficient (Q_T/Rainfall; rainfall that triggered the event is shown in Table 2); Duration is the length of the storm for which the TSS loads are calculated; n_T is the number of turbidity measurements made during the storm (often recorded minutely); T_{max} is maximum recorded turbidity (upper limit of the sensor is 3000 NTU); TSS_{max} is maximum recorded suspended solid concentration; TSS_{load} is the estimated total load for the storm (determined by event-specific variations of Eq. 5); $TSS_{<63\mu m}$, $TSS_{63-2000\mu m}$, and $TSS_{>2000\mu m}$, are the percentages of total TSS load in identified size range.

Table 4. Annual precipitation (P_{annual}), basin runoff (Q_{annual}), runoff coefficient (ROC), total suspended solid load (TSS_{annual}), and basin sediment yield ($Yield_{annual}$) for Mae Sa Catchment during the three year study.

Year	P_{annual} mm	Q_{annual} mm	ROC_{annual} -	TSS_{annual} Mg	$Yield_{annual}$ Mg km^{-2}	Uncertainty %
2006	1934	795	0.41	62235	839	-28 to 39
2007	1632	552	0.34	23922	323	-33 to 43
2008	1663	414	0.25	11890	160	-33 to 38

ROC = (Q_{annual}/P_{annual}). Uncertainty values pertain to the TTS load and yields. They are interpreted as the following: for example, the year 2006 TSS_{annual} value of 62235 Mg may be overestimated by 28% or underestimated by 39%.

Table 5. Parameters of TSS equations for 18 individual storms.

Event/date	a	b	c	d	e	f	ME	Uncertainty (%)
060724	9.91	0.65	103.57	2.16	0.08	1.31	0.98	±26
060728	9.96	0.58	99.23	0.07	0.99	1.28	0.96	±27
060808	17.32	0.33	15.06	2.67	0.11	1.27	0.97	±29
060908	9.96	0.58	98.41	1.64	0.002	1.74	0.96	±28
060909	9.71	0.65	99.85	0.22	1.15	1.20	0.98	±26
060912	9.96	0.58	99.67	0.00	1.14	1.79	0.77	±34
070504	11.02	0.56	179.03	1.02	2.42	0.66	0.79	±36
070614	11.03	0.43	347.65	0.68	0.00001	2.51	0.85	±35
070709	10.00	0.61	355.95	0.80	0.04	1.31	0.73	±33
070822	11.02	0.53	178.88	1.59	0.09	1.27	0.98	±36
070823	10.97	0.70	179.86	0.97	0.78	1.10	0.64	±39
070828	10.94	0.66	178.73	1.34	0.001	1.95	0.95	±37
080519	9.90	0.55	178.35	1.13	0.01	1.59	0.96	±36
080523	9.93	0.56	178.33	1.37	0.0004	2.02	0.91	±36
080603	9.93	0.50	178.45	1.70	0.11	1.21	0.98	±37
080605	9.92	0.41	99.89	0.90	0.00001	2.64	0.99	±39
080610	9.92	0.47	178.95	0.20	0.07	1.36	0.96	±38
080611	9.93	0.50	99.78	1.00	0.00002	2.48	0.63	±41

Event/date reflects year, month, day. The TSS equations related to these parameters follow the form of Equation 8.). Total suspended solid loads estimated using these parameters are listed in Table 3. ME is model efficiency (Equation 1). Uncertainty values are associated with the load estimates in Table 3.

HIGHLIGHTS

* This is the most comprehensive TSS estimation for a SE Asian stream to date.

* Uncertainty ranges are determined for each estimate.

* The complex linkages between TSS and turbidity are explored at several time scales.

* A method is outlined for estimating very high TSS from turbidity and Q measurements.

* TSS is divided into two fractions, for which the largest is not well estimated with turbidity.